Spatial O-GalNAc glycoproteomics atlas: region-specific regulation across the mouse brain

Supplementary Notes:

This Supplementary Information provides additional methodological details and extended analyses supporting the Nature Communications manuscript "Spatial O-GalNAc glycoproteomics reveals region-specific regulation across the mouse brain". It includes Supplementary Figures 1–10, which describe the GlycoDIA 2.0 workflow, including generation of the non-redundant spectral library, the unambiguous O-glycosylation site localization by ETD MS/MS (Supplementary Note 1), and characterization of the O-GalNAc spectral reference library. Supplementary Figures 11–18, together with Supplementary Notes 2 and 3, provide extended protein-centric and comparative analyses, offering additional insights into the spatial regulation of O-GalNAc glycosylation across mouse brain compartments.

Table of Content:

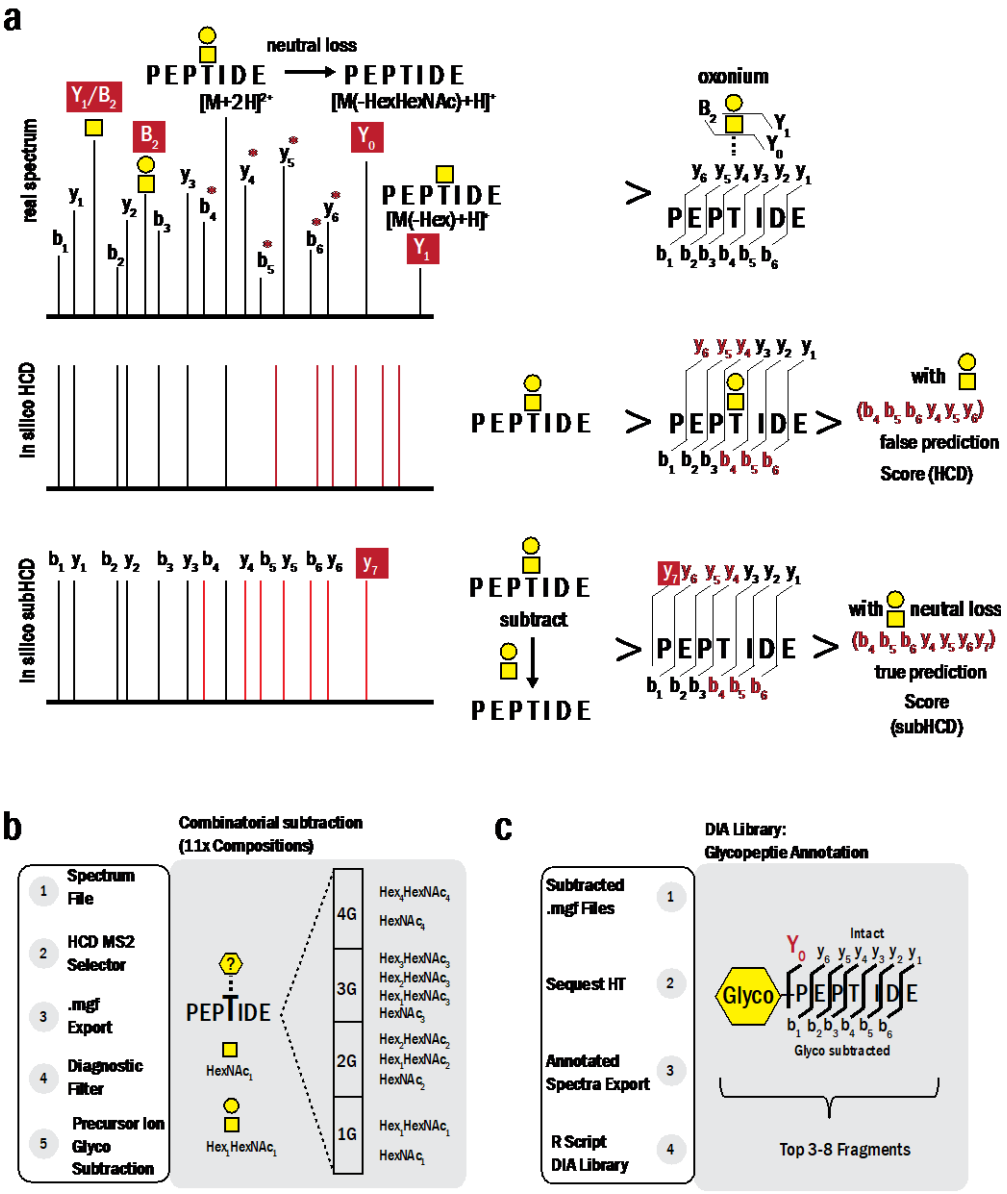

Supplementary Fig. 1. **Non-redundant Glyco-DIA 2.0 library design**. (**a**) closed DDA HCD searching vs. glyco subtracted searching strategy. Comparison between fragment ions annotation in real MS/MS spectrum and in silico match between standard search (in silico HCD) and subtracted glyco strategy (in silico subHCD). (**b**) Glycan combinatorial subtraction applied to HCD MS/MS data to resolve glycopeptide compositions, minimize redundancy and increase identification rate. (**c**) Terminal cumulative glyco design to build the non-redundant Glyco-DIA library.

a

XCorr	5.22				2.81			
Fragment, ppm	b+	b++	y+	y++	b+	b++	y+	y++
1	-	-	-	-	-	-	-	-
2	+0.79	-	-	-1.88	-	-	-	-
3	-1.39	-	-0.62	-1.61	-	-	-	-
4	-1.58	-	-0.44	-1.84	-	-	+0.93	-
5	-	-	-0.85	-1.90	-	-	-0.85	-1.90
6	-1.56	-	-0.79	-0.95	-	-	-0.79	-0.95
7	-1.40	-	-1.15	-1.88	-	-	-1.15	-1.88
8	-1.80	-	-1.86	-	-	-	-1.86	-
9	-1.50	-	-1.84	-	-	-	-1.84	-
10	-0.92	-	-1.87	-	-	-	-1.87	-
11	+1.75	-	-1.34	-	-	-	-1.34	-
12	-	-	-2.07	-	-	-	-2.07	-
13	-2.98	-	-0.83	-	-	-	-0.83	-
14	-		-1.76	-	-	-	-1.76	-
Ions Pos	subHCD-Non Redundant				HCD-Redundant			

b

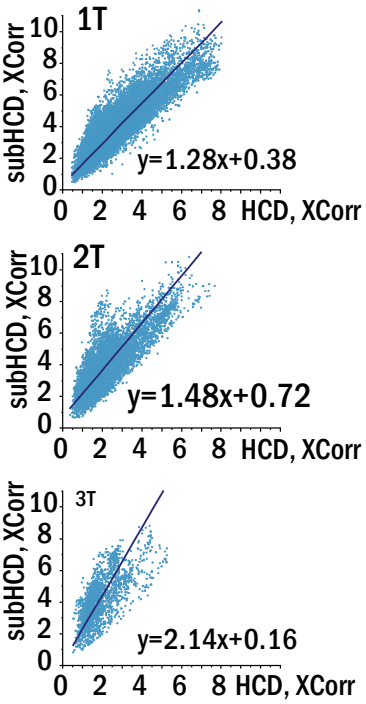

c

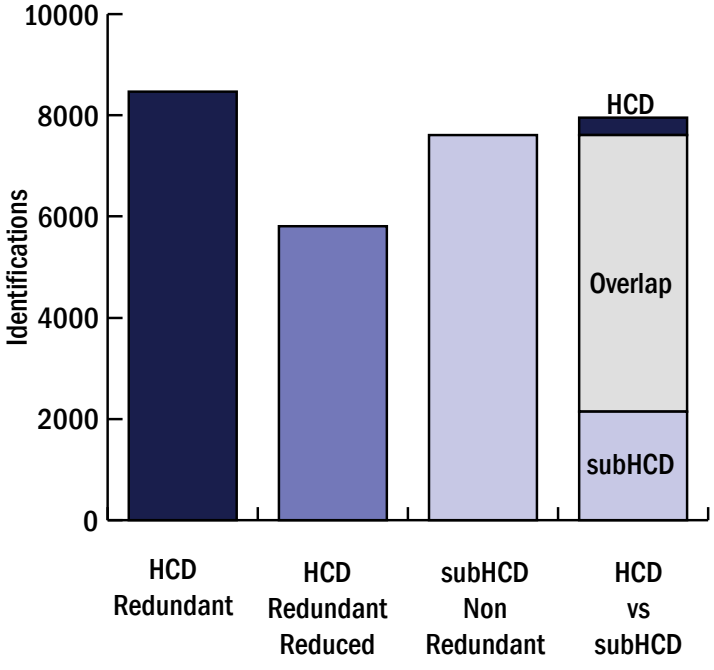

Supplementary Fig. 2. subHCD DDA non-redundant search vs HCD DDA redundant search. (**a**) Precursor ions at m/z 725.6792, z=3 HCD MS/MS spectrum annotation using two different searching strategies: subHCD non redundant (left) with the identification score XCorr=5.22 and standard default redundant (right) with the identification score XCorr=2.81. Precursor ions are identified as SAISSTHIAVTMAR glycopeptide with two core-1 T glycans. (**b**) XCorr correlation between subHCD and standard HCD searching strategies. Data is presented for three identification subsets: monoglycoyslated 1T and polyglycosylated with 2T and 3T, showing in average higher score for subHCD with the increasing trend for more glycosylated peptides. (**c**) Bar plot of the total glycopeptide identifications from the deep HCD DDA analysis of the 8 High pH fractions of glyocopeptides enriched from the whole mouse brain. Same data using standard HCD (redundant) search, standard HCD (redundant) but duplicate removal, subHCD (non-redundant). Stacked bar plot of the comparison between HCD and subHCD searching strategy results.

a

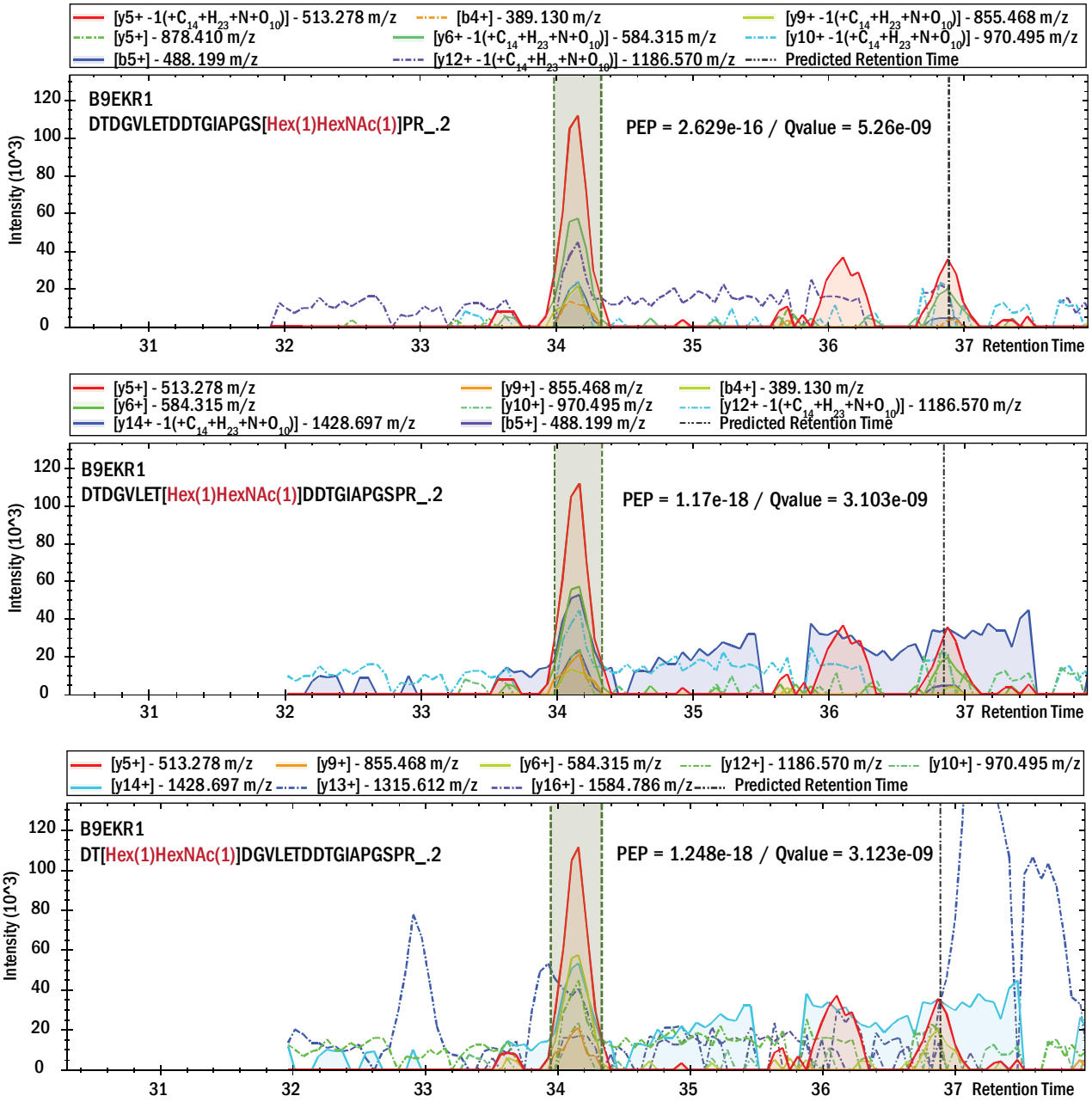
[y5+ -1(+C14+H23+N+O10)] - 513.278 m/z
[b4+] - 389.130 m/z
[y9+ -1(+C14+H23+N+O10)] - 855.468 m/z
[y5+] - 878.410 m/z
[y6+ -1(+C14+H23+N+O10)] - 584.315 m/z
[y10+ -1(+C14+H23+N+O10)] - 970.495 m/z
[b5+] - 488.199 m/z
[y12+ -1(+C14+H23+N+O10)] - 1186.570 m/z
Predicted Retention Time
B9EKR1
DTDGVLETDDTGIAPGS[Hex(1)HexNAc(1)]PR_.2
PEP = 2.629e-16 / Qvalue = 5.26e-09
Intensity (10^3)
Retention Time
[y5+] - 513.278 m/z
[y9+] - 855.468 m/z
[b4+] - 389.130 m/z
[y6+] - 584.315 m/z
[y10+] - 970.495 m/z
[y12+ -1(+C14+H23+N+O10)] - 1186.570 m/z
[y14+ -1(+C14+H23+N+O10)] - 1428.697 m/z
[b5+] - 488.199 m/z
Predicted Retention Time
B9EKR1
DTDGVLET[Hex(1)HexNAc(1)]DDTGIAPGSPR_.2
PEP = 1.17e-18 / Qvalue = 3.103e-09
Intensity (10^3)
Retention Time
[y5+] - 513.278 m/z
[y9+] - 855.468 m/z
[y6+] - 584.315 m/z
[y12+] - 1186.570 m/z
[y10+] - 970.495 m/z
[y14+] - 1428.697 m/z
[y13+] - 1315.612 m/z
[y16+] - 1584.786 m/z
Predicted Retention Time
B9EKR1
DT[Hex(1)HexNAc(1)]DGVLETDDTGIAPGSPR_.2
PEP = 1.248e-18 / Qvalue = 3.123e-09
Intensity (10^3)
Retention Time

b

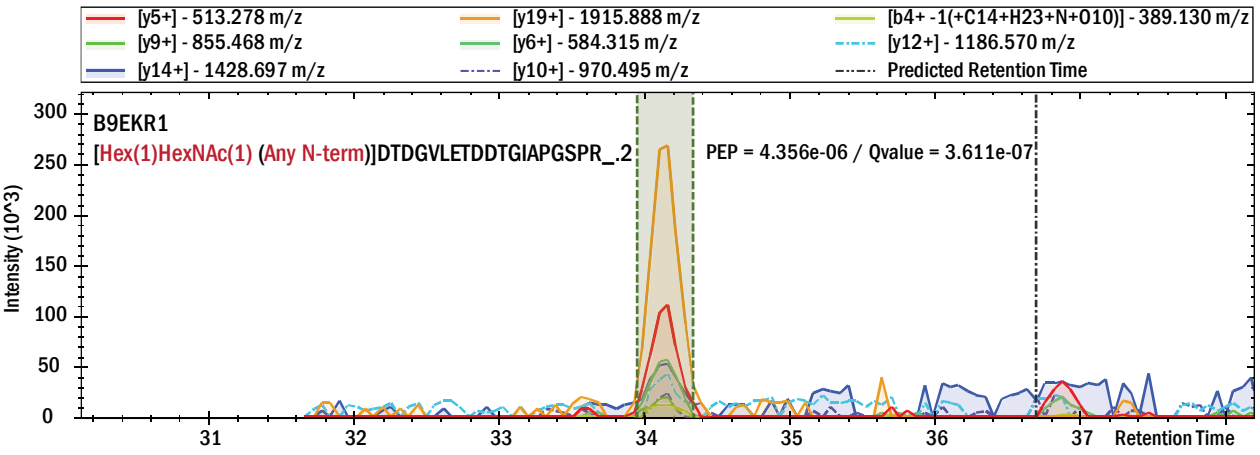
[y5+] - 513.278 m/z
[y19+] - 1915.888 m/z
[b4+ -1(+C14+H23+N+O10)] - 389.130 m/z
[y9+] - 855.468 m/z
[y6+] - 584.315 m/z
[y12+] - 1186.570 m/z
[y14+] - 1428.697 m/z
[y10+] - 970.495 m/z
Predicted Retention Time
B9EKR1
[Hex(1)HexNAc(1) (Any N-term)]DTDGVLETDDTGIAPGSPR_.2
PEP = 4.356e-06 / Qvalue = 3.611e-07
Intensity (10^3)
Retention Time

Supplementary Fig. 3. **Glyco-DIA (redundant) and Glyco-DIA 2.0 (non-redundant) examples.** Precursor ions at m/z 1141.014, z=2 assigned to monoglycosylated (1T) DTDGVLETDDTGIAPGSPRHCD glycopeptide. (**a**) Three different positional isoforms with the glycosylation at Thr2, Thr8 and Ser17 are falsely proposed at the same retention time by Spectronaut using redundant Glyco-DIA approach, whereas true positional isoform would expect different retention time[2]. (**b**) Single non redundant identification is proposed using Glyco-DIA 2.0.

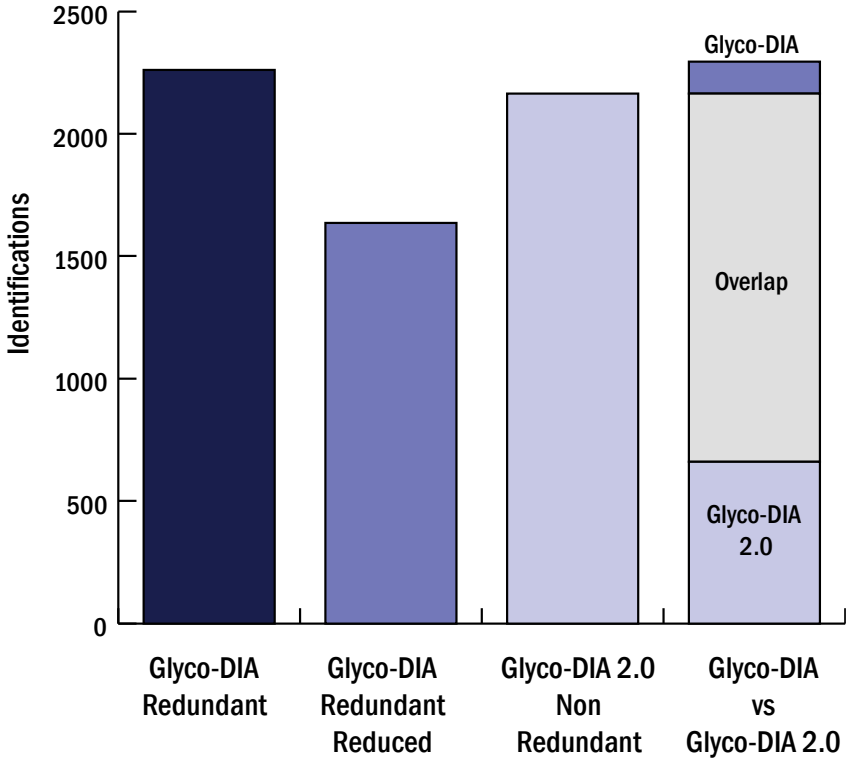

Supplementary Fig. 4. Comparison between Glyco-DIA (redundant) and Glyco-DIA 2.0 (non-redundant) strategies. Bar plot of the total glycopeptide quantification using DIA HCD MS/MS approach from the mouse cerebellum (4 biological replicates). the same data using Glyco-DIA (redundant), Glyco-DIA (redundant) but with duplicate removal and Glyco-DIA 2.0 (non-redundant). Stacked bar plot of the comparison between Glyco-DIA and Glyco-DIA 2.0 strategies.

Supplementary Note 1. Unambiguous glycosylation site mapping by ETD MS/MS

In parallel, we aimed to do an ETD based glycoproteomic analysis of the mouse brain to support our quantitative data with the unambiguous glycosylation site mapping. We performed TMT- based and label free glycoproteomics analysis. For the TMT-based analysis 9 major mouse brain regions (cerebellum, medulla, thalamus, olfactory bulbs, pons, cerebral cortex, midbrain, hippocampus and hypothalamus), together with a control sample (whole brain) were lysed, digested by trypsin and desialylated to remove sialic acid (NeuAc) capping. We employed LWAC enrichment of O-GalNAc glycopeptides using PNA lectin which recognizes T (Galβ1-3GalNAcα-*O*-R) structures (**Supplementary Fig. 5**). We assessed the efficiency of neuraminidase digestion by monitoring oxonium fragment ions characteristic for sialylated glycopeptides, i.e. by extracting *m/z* 274.09 in HCD-MS2 corresponding to the oxonium ion mass of NeuAc following loss of H_2O. Reassuringly, the extracted HCD-MS2 profiles demonstrated significantly reduced presence of NeuAc allowing us to data mine without considering NeuAc modifications on T structures. The elution fractions from PNA LWAC were pooled and further fractionated by high pH fractionation and then analyzed. Additionally, we have analyzed non labeled whole brain enriched with LWAC (Jacalin lectin) and combined two data sets to be used in the Glycoprotein Card annotation (**Fig. 3c, glycodb.org**). Localization of glycosites in glycopeptide sequences from the ETD spectra was based on ptmRS node[6] in PD2.2 and a site probability cutoff score of 90% or greater was applied. We identified unambiguously assigned 1999 O-glycosites derived from 556 glycoproteins (**Supplementary Table 1**).

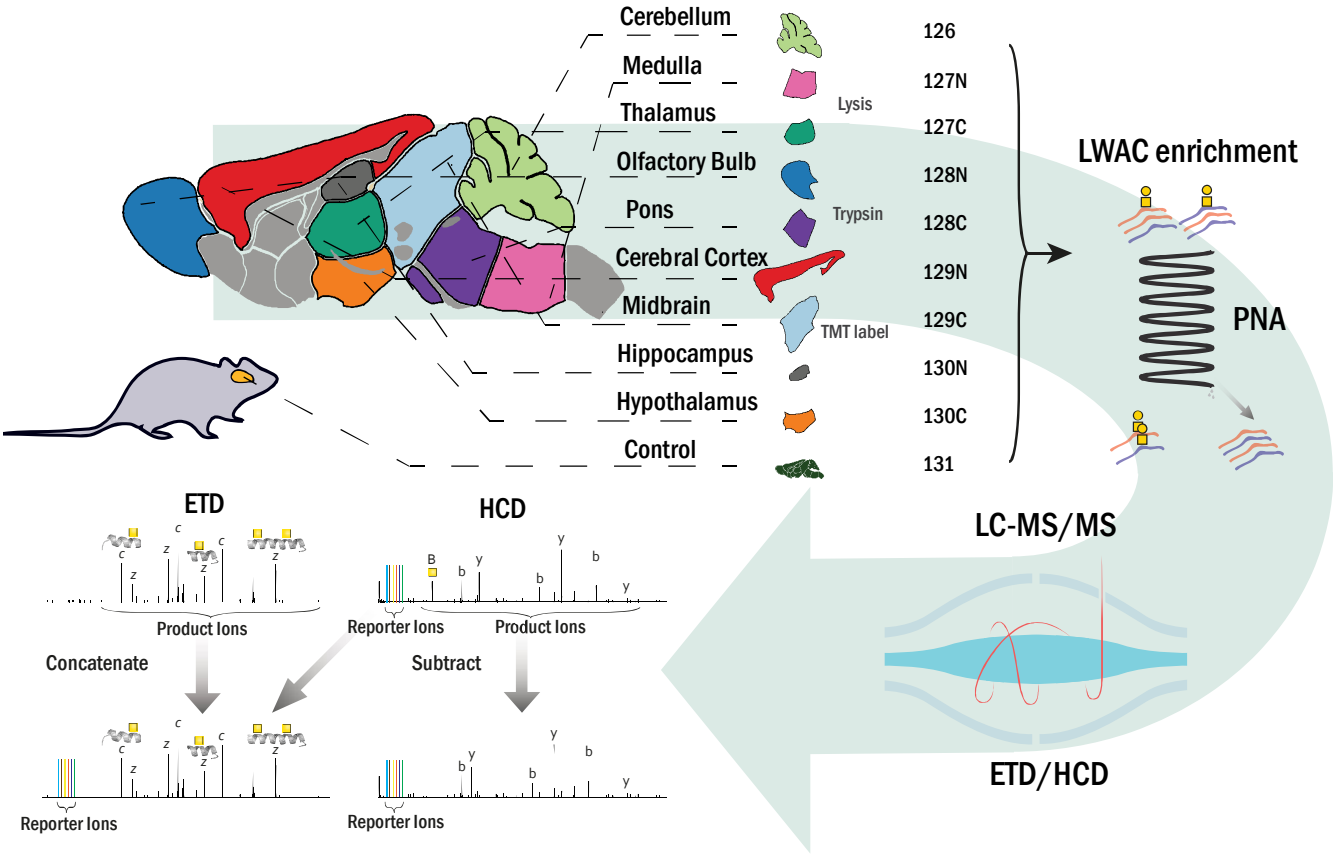

Supplementary Fig. 5. Unambiguous glycosylation site mapping. TMT-multiplexing site-specific glycoproteomic analysis of the mouse brain using ETD MS/MS approach.

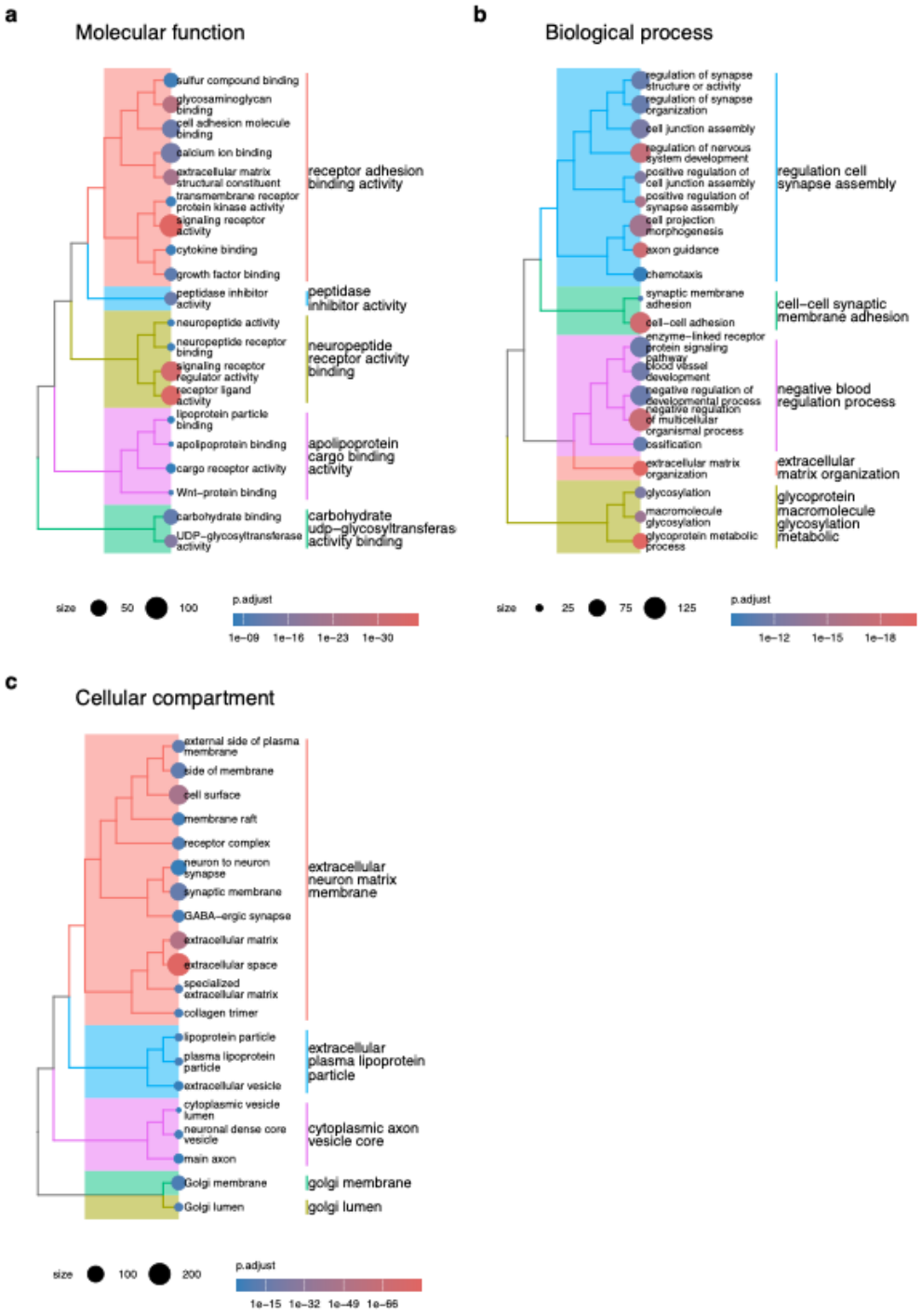

Supplementary Fig. 6. Gene ontology (GO) overrepresentation analysis (ORA) of O-GalNAc DIA library. Top 20 GO terms (by adjusted p-value) were plotted for each GO category. The molecular function (**a**) of O-glycoproteins in the murine brain is dominated by terms in the context of ligand-receptor-mediated interaction, with additional terms such as peptidase inhibitor and neuropeptide activity. O-glycoproteins are overrepresented in a number of biological processes (**b**), mostly related to binding of various signaling molecules. The cellular compartment (**c**) of O-glycoproteins is predominantly the extracellular space as well as the cell surface in general and the synaptic membrane in particular.

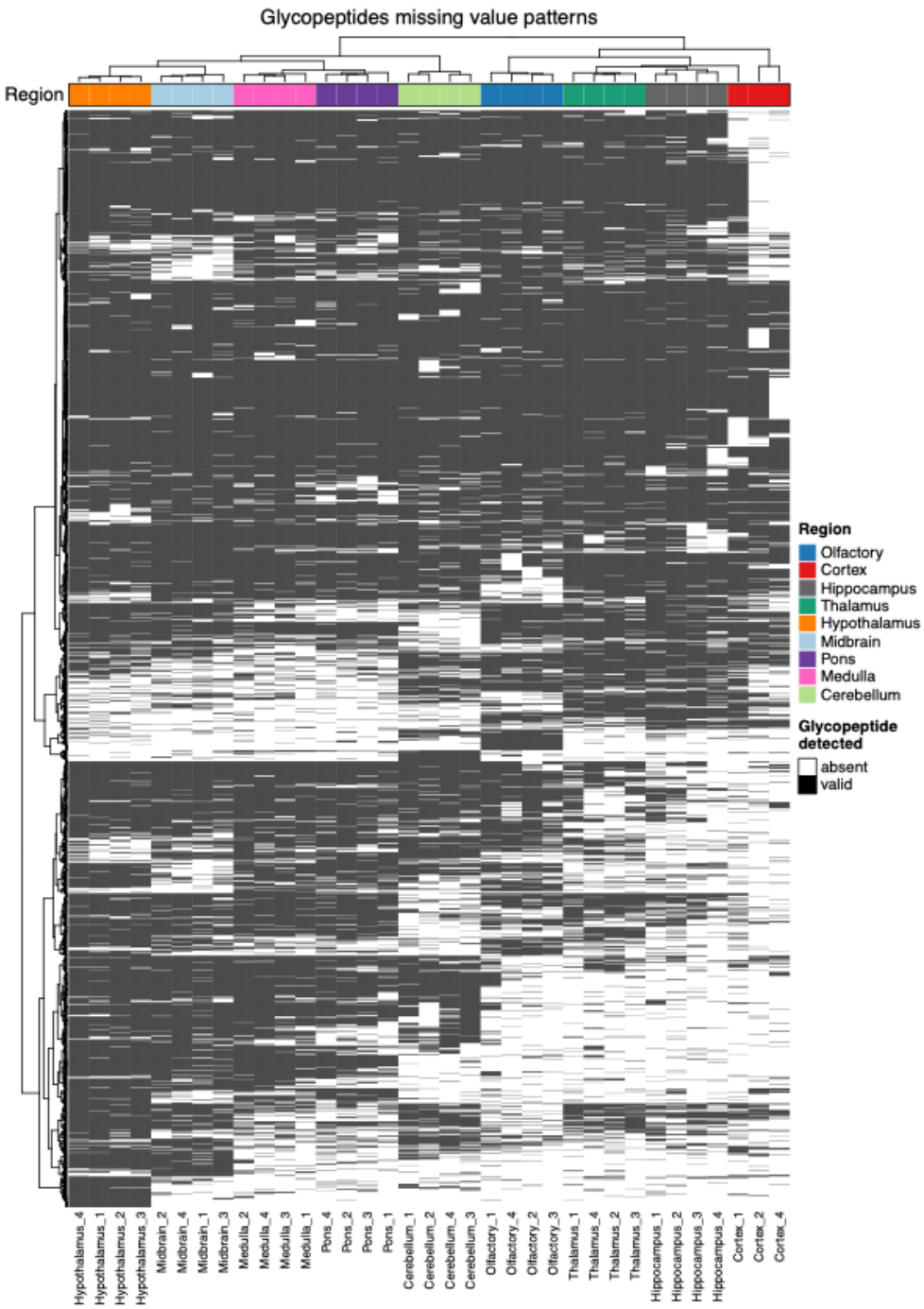

Supplementary Fig. 7. Missing value patterns in glycopeptide data. Quantitative glycopeptide data from all 35 analyzed samples are shown after filtering and before imputation, with samples arranged in columns and glycopeptides in rows. Data were clustered solely based on glycopeptide detection (presence: black; absence: white) in the respective samples regardless of measured abundance. Notably, biological replicates cluster perfectly solely based on missingness patterns, with distinct blocks of present or absent O-glycopeptides across biological replicates of the same brain region. These region-specific patterns suggest that a significant fraction of missing values are missing not at random (MNAR), and likely reflect biologically meaningful differences in tissue specific glycosylation signatures.

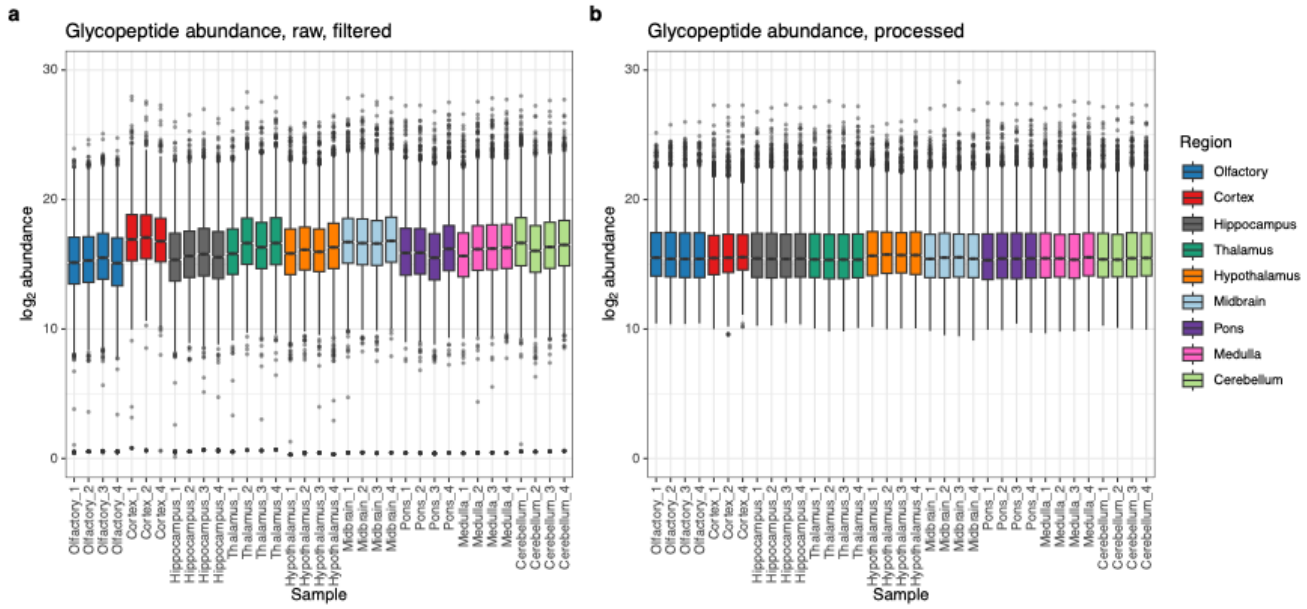

Supplementary Fig. 8. Distribution of glycopeptide abundances before and after data processing. Box and whiskers plots show glycopeptide abundances for each sample before processing (**a**, filtered data) and after normalization, batch correction and missing value imputation (**b**). Boxes represent the interquartile rage (IQR; 25^{th} – 75^{th} percentiles), the center notch indicates the median and whiskers extend to 1.5 × IQR from the median. Values outside the whiskers are plotted as individual points.

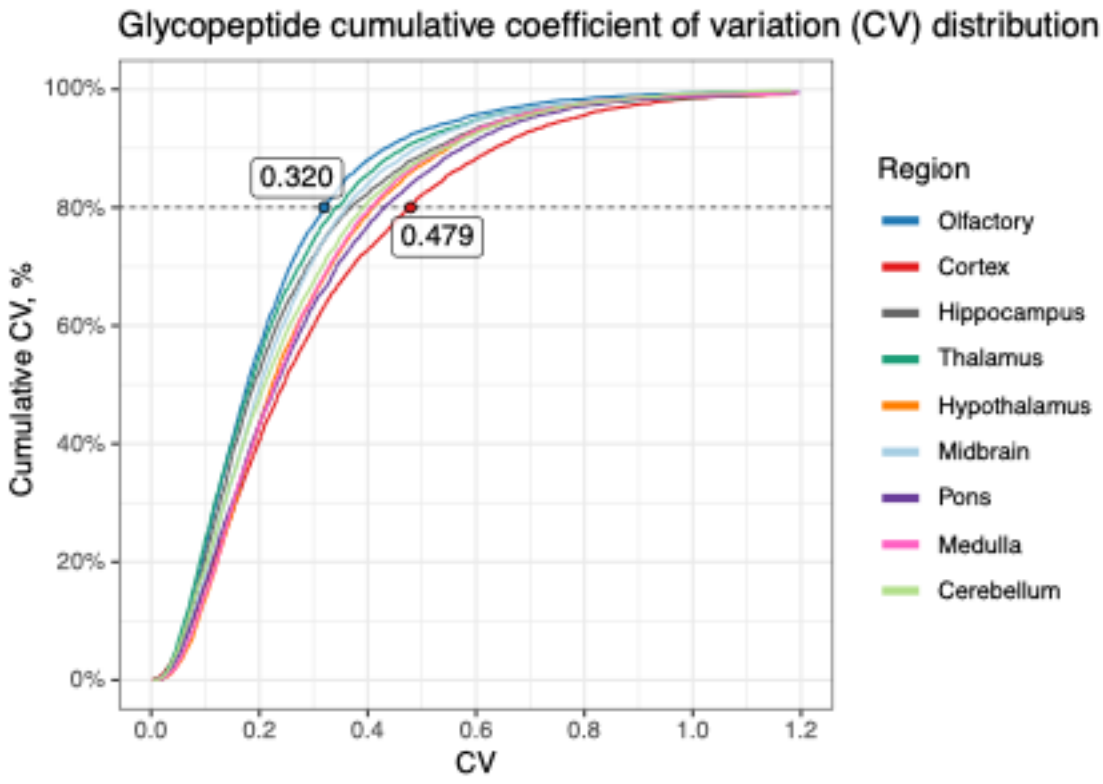

Supplementary Fig. 9. Cumulative distribution of glycopeptide abundancies coefficient of variation (CV) by brain region. The cumulative fraction of quantified glycopeptide abundances per brain region is plotted against increasing CV (the intra-region standard deviation divided by mean abundance). Data quality varied across regions, with olfactory bulb showing lowest variability (80% of values with CV < 0.320), whereas the data obtained from cerebral cortex exhibit the highest variability (80% of values with CV < 0.479).

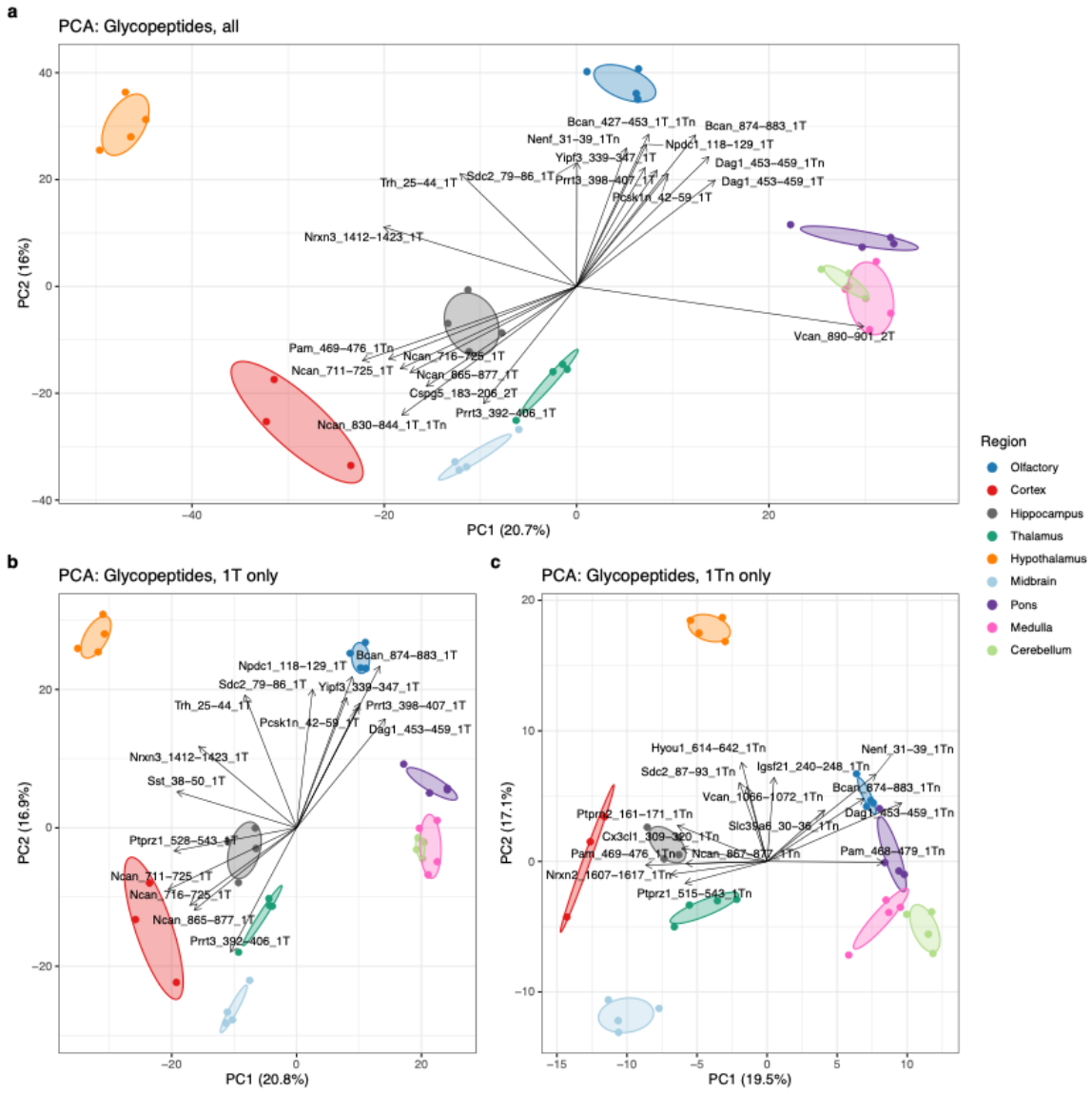

Supplementary Fig. 10. Principal Component Analysis (PCA) of regional glycopeptide abundance data. Dimensionality reduction of the complete glycopeptide abundance data after processing using PCA (**a**) revealed four major regional groups: hypothalamus, olfactory bulb, cortex-hippocampus-thalamus-midbrain and pons-medulla-cerebellum. The pons-medulla-cerebellum samples are clustered tightly with a substantial overlap between regions. The cortex, hippocampus, thalamus and midbrain samples clusters are distinct but show sub-grouping. Of note, these grouping broadly reflect the spatial organization and biological function of the murine brain. Interestingly, while the PCA visualization of complete data and glycopeptide abundancies limited to peptides harboring the 1T glycans are largely identical (**b**), the analysis based on just peptides with the 1Tn glycan (**c**) is different with the olfactory bulb samples clustering close to pons-medulla-cerebellum group. This shift could suggest that regional variation in O-glycosylation might be partly glycan-dependent.

Supplementary Note 2. Summary of O-glycoproteins occupancy regulations across brain regions.

Our dataset comprises both a high-confidence region-resolved O-glycopeptidome as well as the corresponding proteome, both of which are frequently regulated across the mouse brain. Therefore, we next asked how glycopeptide regulation differs systematically between brain compartments and to what extent these changes track the respective proteome. The compartment-resolved O-GalNAc glycoproteomics revealed extensive regional remodeling across the mouse brain, with glycopeptide regulation varying in both magnitude and direction between anatomical compartments. In many comparisons, glycopeptide-level changes did not simply mirror the corresponding proteome response, indicating that spatial variation in O-GalNAc glycosylation cannot be explained solely by differences in total protein abundance (**Fig. 4c**).

To distinguish protein-driven from glycosylation-associated effects, we paired the quantitative glycoproteomics and proteome datasets and compared glycopeptide fold changes with those of the corresponding proteins. More than half of the quantified glycopeptide features could be linked to a quantitative proteome measurement, providing a basis for integrated interpretation of regional regulation (**Fig. 4a**). Pairwise comparison across brain-region combinations revealed that glycopeptide and protein changes followed several distinct regulatory relationships rather than a single common pattern. We therefore classified paired glycopeptide-proteome comparisons into distinct regulatory modes based on the direction and significance of the corresponding changes. In addition to unchanged or non-significant cases, four major classes emerged: concordant regulation, in which glycopeptide and protein changed in the same direction; glycopeptide-specific regulation, in which the glycopeptide changed without a corresponding protein shift; protein-specific regulation, in which the protein changed without a corresponding glycopeptide response; and discordant regulation, in which glycopeptide and protein changed in opposite directions (**Fig 4b, c**).

Representative pairwise comparisons illustrated each of these regulatory modes across brain compartments are shown in **Figure 4c**. As a reference, unchanged or non-significant regulation was observed for amyloid precursor like protein 1 (APLP1) in medulla versus pons comparison, where neither the glycopeptide nor the corresponding proteome feature showed a significant regional shift (**Supplementary Fig. 12**, **glycodb.org**). Concordant regulation was detected for CX3CL1 in the cerebellum with the hippocampus or VGF hypothalamus versus medulla comparisons, where increased glycopeptide signals were accompanied by increased protein abundance (**Fig. 3b, 4c**). Glycopeptide-specific regulation was observed for IGFBP5 in medulla relative to hypothalamus, where glycopeptide abundance changed significantly in the absence of a detectable corresponding protein-level shift (**Fig. 4c**). Protein-specific regulation was exemplified by VGF in cerebellum versus medulla, where the protein

changed significantly without a corresponding glycopeptide shift (**Fig. 4c**). A fourth, less common class was represented by discordant regulation, as observed for CD44 in medulla versus hippocampus comparison, where glycopeptide abundance changed in the opposite direction to the corresponding protein (**Fig. 4c**).

Having established the possible regulatory states resulting from the combination of proteome and O-glycopeptidome level regulation (**Fig. 4b**), we aimed to generate a global overview of the paired data across all 36 unique pairwise comparisons of the nine brain regions. Before examining the regulatory landscape of individual glycoproteins (**Fig. 5**), we first asked whether comparisons exhibiting extensive protein regulation also showed extensive occupancy remodeling. To address this question, we summarized for every regional comparison the number of significantly regulated proteins together with the number of glycoproteins exhibiting protein-independent glycopeptide regulation (Supplementary Fig. 11). Overall, these two parameters were strongly correlated ($R^2 = 0.67$, $P < 0.001$), indicating that regional comparisons involving widespread proteome regulation generally also exhibit extensive remodeling of O-GalNAc occupancy. Notably, the number of glycoproteins displaying protein-independent O-glycopeptide regulation consistently exceeded the number of significantly regulated proteins across all comparisons, suggesting that changes in glycosylation occupancy represent a more prevalent mode of molecular regulation than changes in protein abundance alone. The extent of O-glycopeptide regulation varied substantially between brain-region comparisons. The highest numbers for remodeling O-GalNAc glycosylation within glycoproteins were observed for hypothalamus versus midbrain and cortex versus cerebellum comparisons, each involving 126 glycoproteins, followed by cortex versus olfactory bulb with 118 glycoproteins. In contrast, pons versus medulla, midbrain versus thalamus, and thalamus versus hippocampus showed comparatively limited O-GalNAc remodeling, with 37, 49, and 52 independently regulated glycoproteins, respectively (**Supplementary Fig. 11**). These differences largely reflect the spatial organization of the mouse brain, where anatomically and functionally related compartments display more similar glycosylation regulatory patterns. Nevertheless, several regional comparisons deviated substantially from the overall relationship between protein regulation and glycopeptide alteration, indicating that O-GalNAc occupancy is not simply consequence of protein abundance. The most striking example was the comparison between the hypothalamus and midbrain, which exhibited the highest number of independently regulated O-glycopeptides within 126 glycoproteins despite only 45 proteins being significantly regulated, placing this comparison well above the expected trend (**Supplementary Fig. 11**). Similar deviations were also observed for pons versus cerebral cortex, which displayed extensive glycopeptide-specific regulation despite only moderate protein-level changes. In contrast, comparisons such as medulla versus thalamus showed comparatively

fewer glycoproteins with independently regulated O-glycopeptides relative to the extent of proteome regulation and therefore fell below the regression line (**Supplementary Fig. 11**). Together, these outliers demonstrate that while proteome remodeling and O-GalNAc occupancy regulation are globally coordinated, certain brain-region comparisons undergo disproportionately strong or weak occupancy remodeling. These deviations likely reflect compartment-specific regulation of O-GalNAc glycosylation that cannot be explained by changes in protein abundance alone and therefore support the existence of glycosylation as an additional, independently regulated layer of spatial molecular organization across the mouse brain.

To visualize these regulatory relationships at the level of individual glycoproteins, we summarized all regulatory states across the 36 regional comparisons in Figure 5. In this matrix, each column represents an individual comparison between two brain regions, while each row shows the regulatory data of a single glycoprotein. For each brain region pair, we classified the regulation states in accordance with **Figure 4b** and visualized protein-independent glycopeptide regulation (i.e., O-glycosylation occupancy changes resulting from O-glycopeptide selective regulation in orange and protein specific regulation in dark brown). Comparisons without evidence for independent regulation (i.e., concordant regulation and no significant regulation of neither the protein nor its glycopeptides) are colored grey (**Fig. 5**). The resulting matrix of distinct regulatory state values was ordered with agglomerative hierarchical clustering (using Ward's D2 method to minimize the total within-cluster variance with Euclidean distance). Interestingly, many brain regions could be clustered together solely based on their proteome – O-glycoproteome regulation status, without explicit knowledge of their actual abundance of either protein or its O-glycopeptides. Comparisons involving either hypothalamus, cerebellum or olfactory bulb (top panel from left to right) relative to all other brain regions formed separate clusters, suggesting a distinct glycosylation signature of these compartments (**Fig. 5)**. This observation is consistent with previous analyses, including the positioning of these regions in principle component analysis (PCA) (**Supplementary Fig. 10**).

The second panel from the top (*Independently regulated Glycoproteins*) shows, as a color code scale, the total number of glycoproteins identified in **Supplementary Figure 11** with evidence for independent regulation of O-glycopeptides in each regional comparison (**Fig. 5**). This representation provides a direct visualization of the extent of occupancy remodeling across brain-region pairs and complements the global analysis of proteome-independent glycosylation regulation described above.

The third panel from the top (*Regulated Proteins*) indicates, as color a code scale, the number of significantly regulated proteins at the proteome level for each regional comparison (**Fig. 5**).

The annotation columns on the right summarize regulatory characteristics for each glycoprotein across all 36 regional comparisons. The *Discordant* indicates whether a discordant regulated for glycoprotein was observed in at least one of the 36 comparisons (red bar: protein significantly upregulated while corresponding glycopeptide downregulated or vice versa). Concordant regulation detected in any comparison is depicted by green bar (**Fig. 5**). Generally, concordant regulation is more prevalent compared to discordant. Interestingly, a number of glycoprotein-glycopeptides comparisons show both types of regulation across different compartments. The adjacent column (*Independent regulation*) summarizes the number of comparisons in which changes in glycosylation occupancy were detected as glyco-specific (orange), protein-specific (brown), or no occupancy change (light grey) per glycoprotein. The next column (left to right) indicates the number of comparisons in which there are glycopeptides with no evidence for significant regulation for that glycoprotein in grey (*No regulation*). The last column shows the number of comparisons with significant regulation on protein level in violet (Protein regulation) (**Fig. 5**).

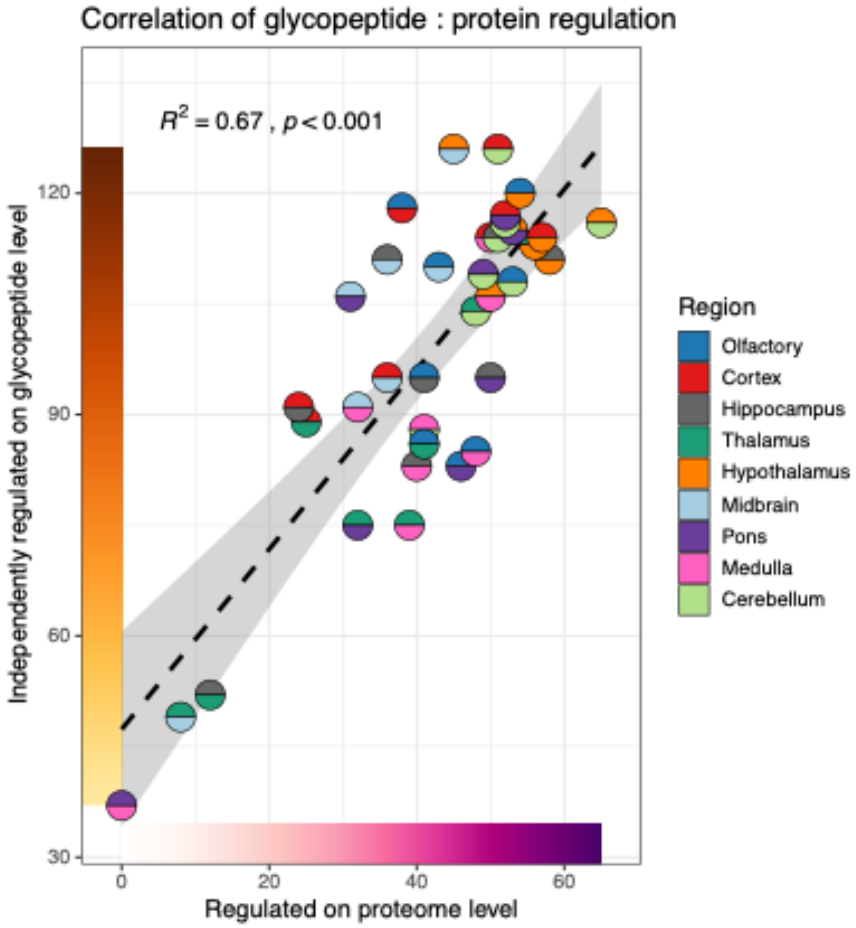

Supplementary Fig. 11. Correlation of glycopeptide and protein regulation. Scatterplot including linear regression of the 36 unique pairwise comparisons of the nine analyzed brain regions are shown as two-colored circles according to the region pair. Position of the region pair on the X-axis shows the number of glycoproteins (out of 280) which are significantly regulated on protein level in that comparison (see also **Fig.5**, "Regulated Proteins" panel), while position along the Y-axis shows the number of proteins with evidence for independent regulation on glycopeptide level (see also **Fig.5**, "Independently regulated glycoproteins" panel). Across regional comparisons, protein-level regulation and glycopeptide changes showed a strong positive correlation (linear regression, $R^2 = 0.67$, $P < 0.001$), indicating that extensive proteome remodeling is generally accompanied by increased O-GalNAc remodeling. However, several comparisons deviated from this overall trend. For example, hypothalamus versus midbrain exhibited disproportionately extensive glycopeptide-level remodeling, with 126 glycoproteins showing protein-independent glycopeptide regulation despite only 45 significantly regulated proteins. Conversely, comparisons such as medulla versus thalamus showed relatively limited O-GalNAc remodeling compared with the proteome regulation, with 75 glycoproteins displaying independent glycopeptide regulation and 39 proteins regulated at the proteome level.

Supplementary Note 3. Intra-protein regulation of O-glycosylation and extended case studies

Beyond global abundance changes, the data also further revealed fine-grained spatial intra-protein regulation at the level of individual glycosylation sites and structural domains, generating brain region-specific glycoproteoforms (**Fig. 6, Supplementary Fig. 13-18**). To facilitate visualization of the intra-protein regulation of O-glycosylation we introduced a positional volcano plot that combines the conventional volcano plot representation of quantitative O-glycopeptide abundance changes between selected brain region pairs with color-coded positions of the corresponding glycopeptides along the protein sequence (**Fig. 6, Supplementary Fig. 12-18**).

To illustrate how positional volcano plots enable functional interrogation of intra-protein O-GalNAc regulation, we selected three representative proteins: CX3CL1 (fractalkine), a neuron-enriched chemokine mediating cell–cell communication; APLP1, a synaptic adhesion protein of the amyloid precursor protein family; and GFRA2, a GPI-anchored neurotrophic co-receptor that mediates RET signaling. These proteins span distinct modes of extracellular signaling while share a common dependence on O-GalNAc glycosylation for modulation of their function.

CX3CL1 (fractalkine) is the single member of CX3C chemokine family that plays a crucial role in neuron communication, homeostasis, synaptic plasticity, and regulation of neuroinflammation responses[8, 9]. CX3CL1 is a transmembrane protein comprising of a processed signal peptide (aa 1-24), actual chemokine domain (aa 25-100), glycosylated mucin-like stalk (aa 101-341), transmembrane domain (aa 342-364), and cytoplasmic tail (aa 365-395) (Uniprot O35188). The mucin-like stalk is shed by constitutively expressed ADAM10 (or inducible ADAM17) within the membrane proximal region with a putative cleavage site(s) near the Arg-Arg (RR) motif at aa 337-338, generating soluble CX3CL1 protein and membrane-retained fragments[8, 9].

Apart from the cortex, hippocampus and thalamus which showed relatively higher CX3CL1 expression levels, we observed only minor variation in total protein levels across other brain regions. However, O-GalNAc glycosylation displayed pronounced intra-protein and compartment-specific distribution of O-glycopeptides within the stalk domain. Based on EDT analyses, we identified O-glycan rich regions adjacent to the chemokine domain (aa109-150: Thr111, Thr115, Thr118, Ser122, Ser124, Thr142 and Thr143) as well as two membrane-proximal regions relative to the transmembrane domain: a distal region (aa 259-309: Ser262, Thr270, Thr281, Ser285, Thr294, Ser302 and Ser304) and a proximal region (aa 309-338: Thr316 and Thr327). Pons and medulla showed preferential enrichment of O-glycosylation in the region adjacent to chemokine domain, whereas midbrain and olfactory bulb exhibited increased glycosylation in the transmembrane-proximal region (**Fig. 6a, Supplementary Fig. 13**, **glycodb.org**). In contrast, cerebellum displayed the lowest overall glycosylation levels, and many comparisons involving

this compartment revealed coordinated or glyco-specific increases in O-GalNAc occupancy at most sites in other brain areas (**Fig. 4c, Supplementary Fig. 14**, **glycodb.org**). Hence, our data revealed that CX3CL1 is not uniformly glycosylated but instead undergoes extensive region-specific remodeling of O-GalNAc occupancy across generating distinct glycoproteoforms. Because proteolytic shedding occurs within the membrane-proximal region, these differences could influence cleavage susceptibility and the balance between membrane-bound and soluble CX3CL[10]. Functionally, heavily glycosylated regions across domains may favor a more extended and structurally constrained stalk that supports stable adhesion and regulated shedding, whereas region-specific patterns may fine-tune ligand accessibility, protease engagement, and chemokine signaling.

GFRA2 (GDNF family receptor α2) is a glycosylphosphatidylinositol (GPI)-anchored cell-surface receptor that mediates signaling by the neurotrophic factor neurturin and, to a lesser extent, GDNF[18]. Upon ligand binding, GFRA2 forms a receptor complex with the RET tyrosine kinase, promoting RET activation and downstream signaling pathways involved in neuronal survival, differentiation, and maintenance[18, 19]. In the mouse brain, GFRA2 (Uniprot O08842) is expressed in multiple neuronal populations and contributes to the development and function of both central and peripheral nervous systems[19]. The mature mouse GFRA2 protein (464 aa) is synthesized in the endoplasmic reticulum, where C-terminal peptides are replaced by a GPI anchor attached to ω-site (Ser443) via the GPI transamidase complex[20, 21]. Following ER processing, lipid remodeling, and Golgi maturation, the receptor acquires glycosylation that concentrated in a low-complexity extracellular stalk region (aa 363–392), which is thought to increase stalk stiffness and regulate special presentation of the GFRA2 ligand-binding D1-D3 domains and at the cell surface[22]. As a component of the neuronal glycocalyx, the O-glycosylated stalk putatively functions as a structural spacer that projects the ligand-binding domains away from the membrane and surrounding proteins, thereby modulate efficient access and ligand-binding[22, 23].

GFRA2 provided a prominent example of brain region-dependent changes in site specific glycosylation. O-GalNAc-modified glycopeptides spanning amino acids 367-378, 383-412 and 423-436 displayed distinct abundance patterns across brain compartments. Cortex, midbrain, thalamus and hypothalamus preferentially showed increased O-GalNAc occupancy within the membrane proximal extracellular stalk region around (aa 423-436), immediately upstream of the GPI-anchor attachment sequence (**Fig. 6b, Supplementary Fig. 15, glycodb.org**). In contrast, pons, medulla, cerebellum, olfactory bulb and, to a less extent, hippocampus exhibited enrichment at membrane distal region adjacent to GFRA2 D3-domain (aa 367-378) (**Fig. 6b, Supplementary Fig. 15, glycodb.org**). These reciprocal shifts frequently occurred without detectable differences in total protein abundance of GFRA2, indicating that glycoform

switching occurs in a region dependent manner independently of changes in protein expression. In a subset of comparisons, however, enrichment of distal glycosylation was accompanied by increased GFRA2 abundance, suggesting that site-specific O-GalNAc occupancy may in some cases contribute to receptor stabilization or reduced turnover. Given the close proximity of these glycosylation sites to the D3 ligand-binding domain, and the GPI-anchor attachment region, differential O-GalNAc occupancy may influence receptor stability, membrane retention, organization within the glycocalyx, and the spatial presentation of ligand-binding surfaces. Such structural changes could alter the positioning of the D3 domain relative to the cellular membrane, thereby modulate ligand accessibility and the assembly of ligand-induced RET signaling complexes. Hence, preferential enrichment of distinct glycoforms across brain compartments suggests that O-GalNAc glycosylation may constitute an additional layer of regulation governing GFRA2 receptor organization and neurotrophic signaling within the neuronal glycocalyx.

APLP1 (amyloid precursor-like protein 1) is a neuron-specific transmembrane cell-adhesion protein that regulates synaptic development, zinc-dependent cell signaling, and protein trafficking[11]. The full-length mouse protein (aa 39–654) comprises a large extracellular domain (aa 39–584), a transmembrane helix (aa 585–607), and a cytoplasmic tail (aa 608–654) (Uniprot, Q03157). APLP1 undergoes regulated proteolysis similar to APP but lacks the Aβ region and therefore does not generate amyloidogenic peptides[11]. Instead, APLP1 is processed predominantly via a non-amyloidogenic α - γ-secretase pathway[12]. Shedding of the extracellular domain, primarily mediated by ADAM10, which cleaves APLP1 to release the soluble Aplp1 (sAPLP1) fragment into the extracellular space[12, 13]. Notably, APLP1 extracellular region contains two conserve domains E1 (aa 50-212) and E2 (aa 297-488). The APLP1 E1 domain mediates zinc-dependent trans-synaptic cell adhesion and extracellular protein interaction, whereas E2 domain contributes to cell adhesion via heparin-induced antiparallel homodimerization to bridge neighboring neurons at the synapse[11, 14-16]. Recently, the E1 domain was shown to bind the lymphocyte-activation gene 3 (LAG3), forming a receptor complex that actively promote the internalization of toxic alpha-synuclein aggregates into healthy neurons and to drive Parkinson's disease progression and neurodegeneration[17]. Secretases mediated cleavage release entire soluble sAPLP1 ectodomain retains both the E1 and E2 domains[12] that can function as a decoy receptor which captures and sequesters free alpha-synuclein in the extracellular space and potentially protecting against neuronal death[17].

Our data reveals pronounced intra-protein specific remodeling of APLP1 O-glycosylation across brain compartments. We identified O-glycopeptides throughout APLP1 extracellular domain with the strongest regional differences observed between glycopeptides adjacent to the E1 domain (aa 201-229),

to the E2 – proximal region (aa 272-287) and to two membrane proximal regions adjusted to transmembrane domain (aa 520-541 and 541-553) indicating pronounced site- and domain-specific O-GalNAc remodeling across brain compartments (**Fig. 6c, Supplementary Fig. 16-18**). Compared with the pons, medulla, and cerebellum, the hypothalamus and hippocampus exhibited increased abundance of O-glycopeptides adjacent to the E1 and/or E2 domains, whereas glycopeptides proximal to transmembrane domain were enriched in pons, medulla, and cerebellum (**Fig. 6c, Supplementary Fig. 16**, **glycodb.org**). Accordingly, no significant differences in either protein abundance or glycosylation were observed in comparisons of the pons with the medulla or cerebellum (**Supplementary Fig. 12, glycodb.org**). APLP1 protein abundance varied only modestly across brain regions, with the highest expression in the cerebral cortex and lowest in the cerebellum (**glycodb.org**). Consequently, the cerebral cortex and cerebellum comparison largely reflected concordant regulation of protein abundance and O-glycopeptide levels (**Supplementary Fig. 17**). Most other brain region comparisons were mostly dominated by compartment-specific remodeling of APLP1 glycoproteoforms. For example, comparison of the cerebral cortex and medulla revealed selective intra-protein remodeling, with O-GalNAc occupancy changes restricted to glycosylation sites within the E1 and E2 domains despite only modest non-significant differences in protein abundance (**Supplementary Fig. 18**). The preferential remodeling of glycosylation adjacent to domains involved in extracellular interactions and proteolytic processing suggests that individual APLP1 glycoproteoforms may exhibit distinct biochemical and functional properties. Given the emerging role of APLP1 in alpha-synuclein pathology, these findings raise the possibility that region-specific O-GalNAc glycosylation contributes to the spatial regulation of APLP1 function and may influence mechanisms underlying neurodegeneration[17].

Together, these extended examples demonstrate that brain region specific O-GalNAc glycosylation extends beyond changes in protein abundance and global glycosylation occupancy to involve spatial remodeling within individual protein structures. Distinct extracellular domains and glycosylation sites within individual proteins are selectively regulated in different anatomical compartments, generating region specific glycoproteoforms with the potential to differentially influence protein shedding, ligand recognition, receptor organization and cell–cell communication. Our findings suggest that the spatial organization of O-GalNAc glycosylation within proteins represents an additional regulatory layer of molecular diversity in the brain that complements transcriptional and proteomic heterogeneity and provides a novel mechanistic framework for understanding compartment specific glycoprotein functions.

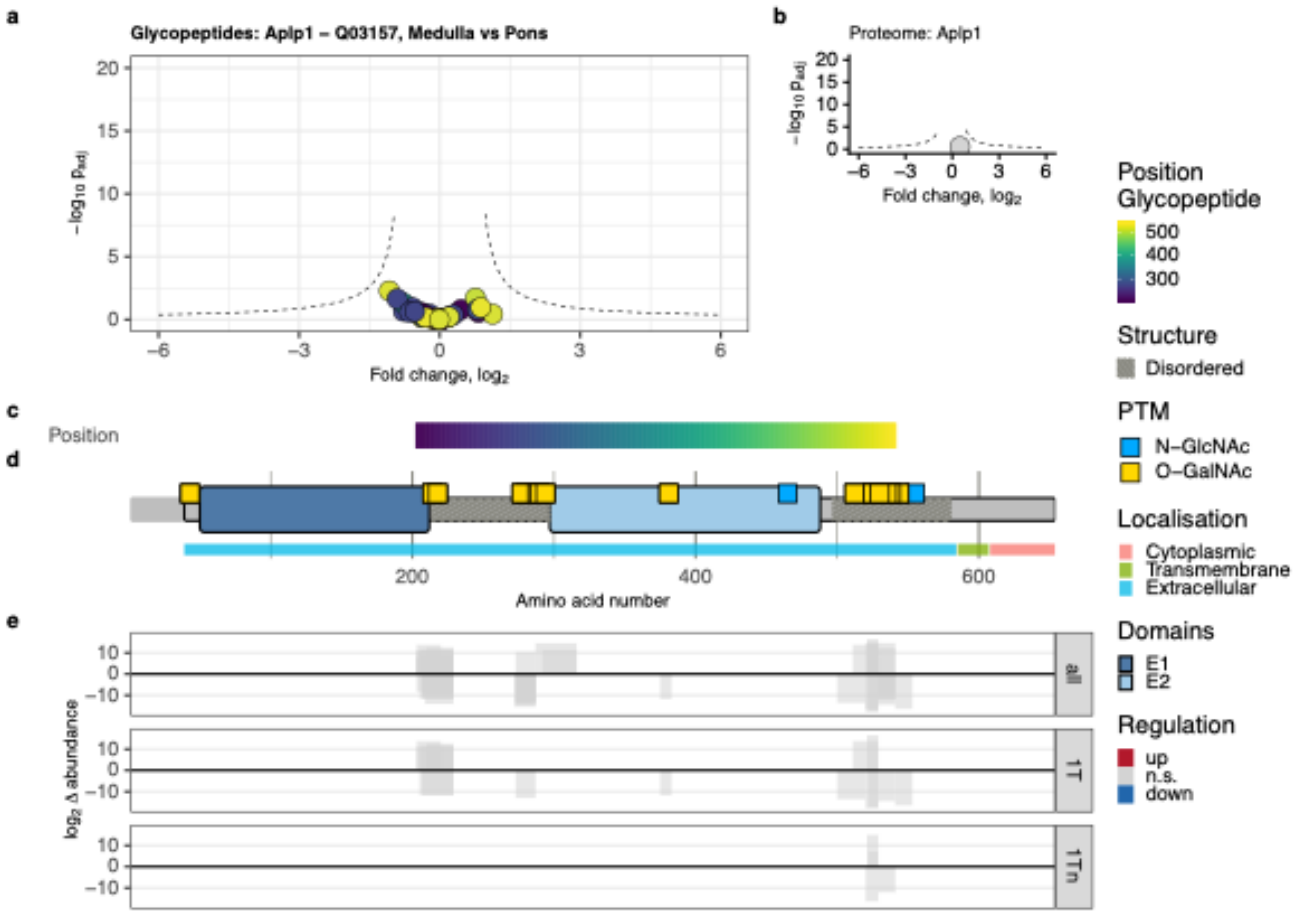

Supplementary Fig. 12. No- regulation of APLP1 O-glycosylation between medulla and pons.

(**a**) Positional volcano blot showing differential abundance of individual O-glycopeptides from APLP1 (Uniprot Q03157) between the medulla and pons. The x-axis represents the $\log_2$ fold change, and the y-axis the $-\log_{10}$ adjusted P value. Each circle corresponds to a quantified O-glycopeptide and is color-coded according to its position within the protein sequence where modifications are localized. Dashed lines indicate significance and fold-change thresholds. (**b**) Conventional proteome volcano plot showing that the overall abundance of APLP1 protein is not significantly altered between the two brain regions. (**c**) Color scale indicating the relative amino acid position of quantified O-glycopeptides along the protein sequence. (**d**) Linear schematic representation of APLP1 protein illustrating annotated structural features including N-GlcNAc (Uniprot Q03157) and mapped O-GalNAc glycosylation sites. O-glycosylation and N-glycosylation sites are shown as yellow and blue squares, respectively, the disordered region is indicated by grey hatching. E1 and E2 domains are drawn as blue and light blue squares, respectively. The extracellular, transmembrane and cytoplasmic regions are indicated below as color lines. (**e**) Position-resolved abundance changes of O-glycopeptides mapped onto the protein sequence. Bars represent $\log_2$ abundance changes between medulla and pons for all quantified O-glycopeptides ("all") and for glycopeptides carrying 1T-core or 1Tn-antigen O-glycan modifications. Grey indicates non-significant regulation. Our analysis of APLP1 glycosylation showed no changes in O-glycopeptides abundance between medulla and pons brain regions across protein domains.

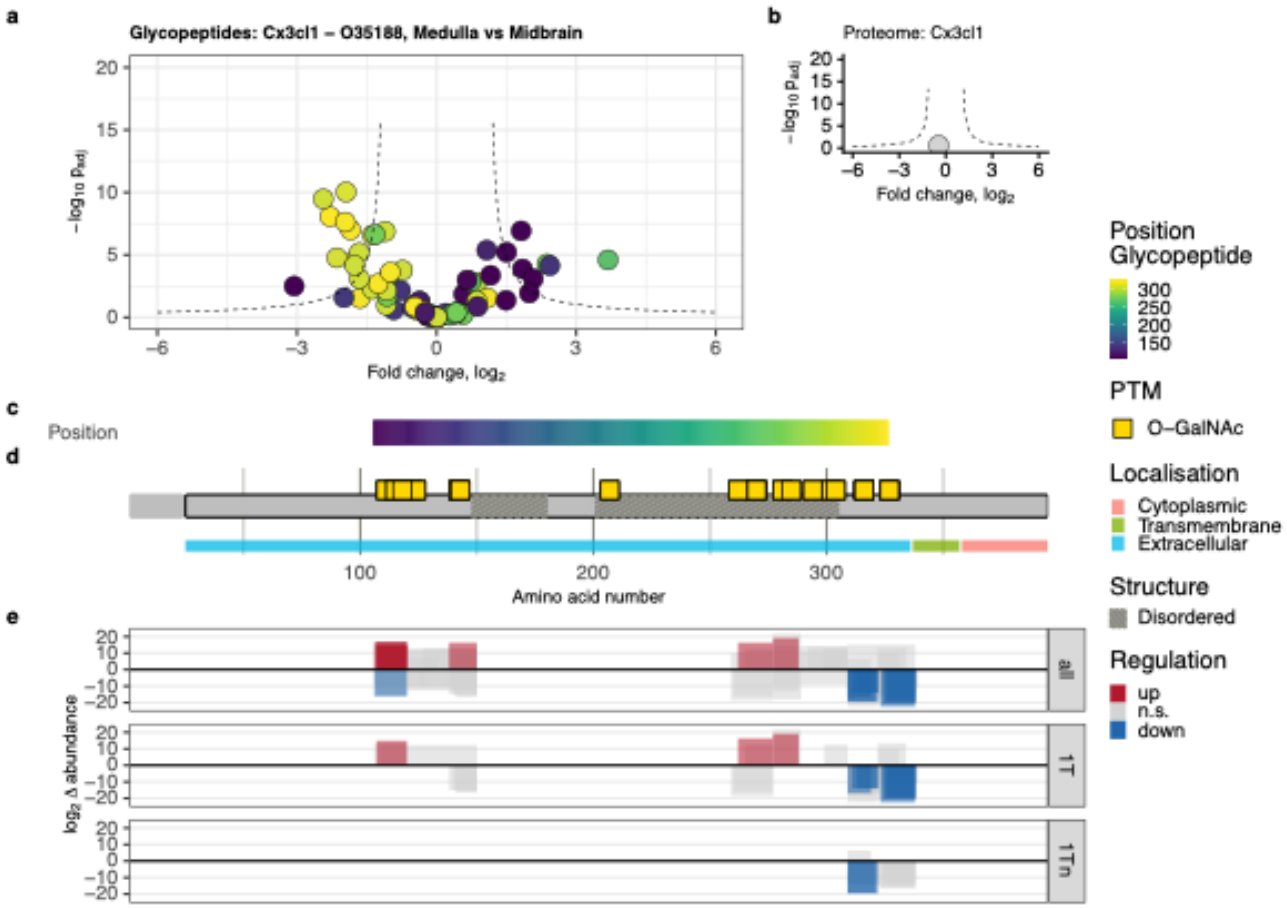

Supplementary Fig. 13. Position-specific regulation of CX3CL1 O-glycosylation between medulla and midbrain. (**a**) Positional volcano blot showing differential abundance of individual O-glycopeptides from CX3CL1 (Uniprot: O35188) between medulla and midbrain. The x-axis represents the $\log_2$ fold change, and the y-axis the $-\log_{10}$ adjusted P value. Each circle corresponds to a quantified O-glycopeptide and is color-coded according to its position within the protein sequence where modifications are localized. Dashed lines indicate significance and fold-change thresholds. (**b**) Conventional proteome volcano plot showing that the overall abundance of CX3CL1 protein is not significantly altered between the two brain regions, indicating that site-specific glycosylation changes occur independently of changes in total protein abundance. (**c**) Color scale indicating the relative amino acid position of quantified O-glycopeptides along the protein sequence (mucin-like stalk). (**d**) Linear schematic representation of CX3CL1 protein illustrating annotated structural features (Uniprot: O35188) and mapped O-GalNAc glycosylation sites. O-glycosylation sites are shown as yellow squares, the disordered region is indicated by grey hatching. The extracellular, transmembrane and cytoplasmic regions are indicated below as color lines. (**e**) Position-resolved abundance changes of O-glycopeptides mapped onto the protein sequence. Bars represent $\log_2$ abundance changes between medulla and midbrain for all quantified O-glycopeptides ("all") and for glycopeptides carrying 1T-core or 1Tn-antigen O-glycan modifications. Red indicates increased abundance, blue decreased abundance, and grey non-significant regulation. The positional volcano blot and positional mapping reveal region-specific intra-protein regulation of CX3CL1 O-glycosylation, generating distinct brain region-specific glycoproteoforms despite no changes in total protein abundance. We observed preferential enrichment of O-glycosylation with regions distal to transmembrane and adjacent to chemokine domain in medulla, whereas midbrain exhibited increased glycosylation in the transmembrane-proximal region.

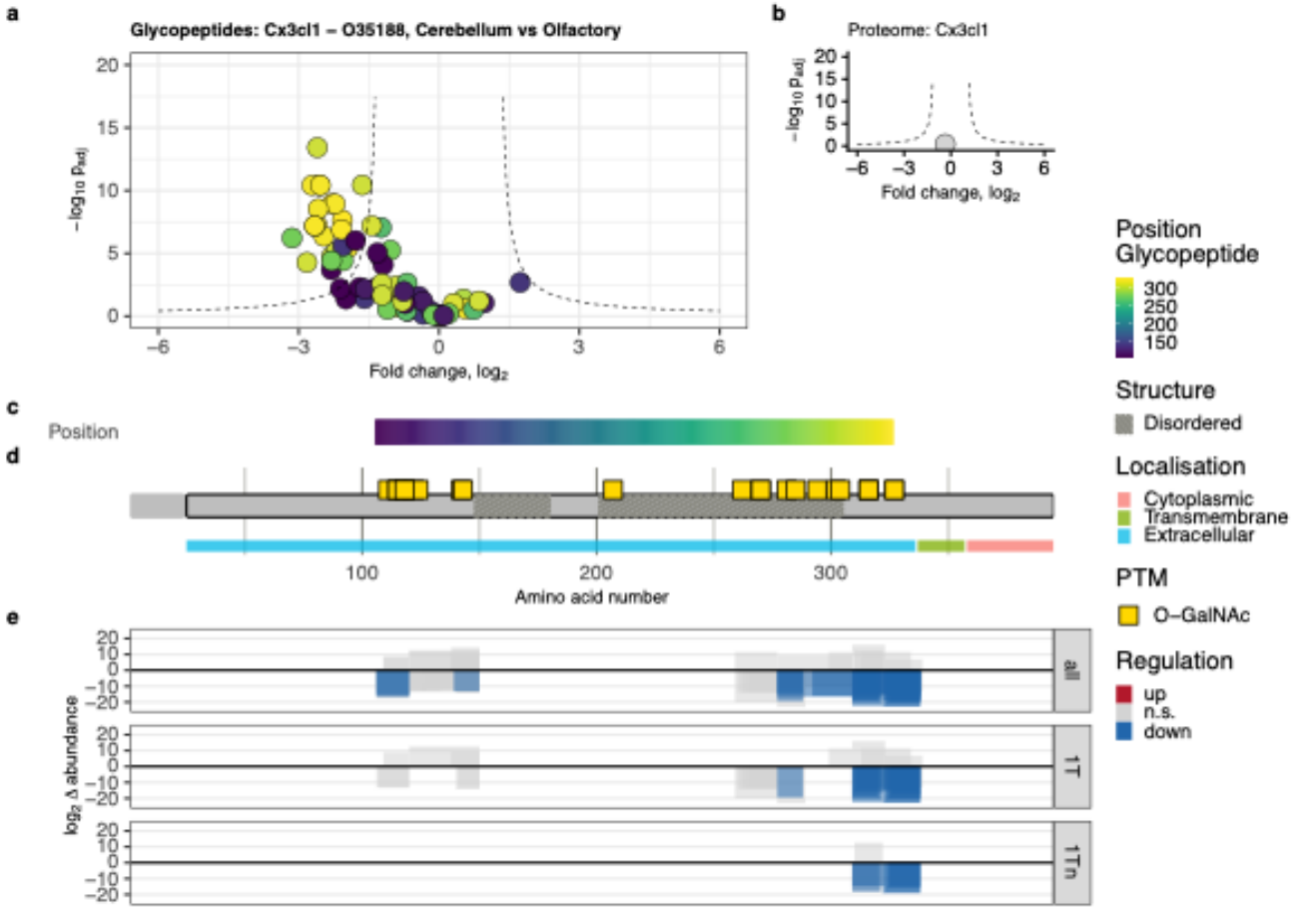

Supplementary Fig. 14. Glyco-specific regulation of CX3CL1 O-glycosylation between cerebellum and olfactory bulb. (**a**) Positional volcano blot showing differential abundance of individual O-glycopeptides from CX3CL1 (Uniprot O35188) between cerebellum and olfactory bulb. The x-axis represents the $\log_2$ fold change, and the y-axis the $-\log_{10}$ adjusted P value. Each circle corresponds to a quantified O-glycopeptide an is color-coded according to its position within the protein sequence where modifications are localized. Dashed lines indicate significance and fold-change thresholds. (**b**) Conventional proteome volcano plot showing that the overall abundance of CX3CL1 protein is not significantly altered between the two brain regions, indicating that site-specific glycosylation changes occur independently of changes in total protein abundance. (**c**) Color scale indicating the relative amino acid position of quantified O-glycopeptides along the protein sequence (mucin-like stalk). (**d**) Linear schematic representation of CX3CL1 protein illustrating annotated structural features (Uniprot O35188) and mapped O-GalNAc glycosylation sites. O-glycosylation sites are shown as yellow squares, the disordered region is indicated by grey hatching. The extracellular, transmembrane and cytoplasmic regions are indicated below as color lines. (**e**) Position-resolved abundance changes of O-glycopeptides mapped onto the protein sequence. Bars represent $\log_2$ abundance changes between cerebellum and olfactory bulb for all quantified O-glycopeptides ("all") and for glycopeptides carrying 1T-core or 1Tn-antigen O-glycan modifications. Blue indicates decreased abundance, and grey non-significant regulation. In cerebellum, Cx3cl1 displayed the lower overall glycosylation levels compared to olfactory bulb independent of intra-protein position of the detected glycopeptide, even though the protein itself appeared to be not regulated.

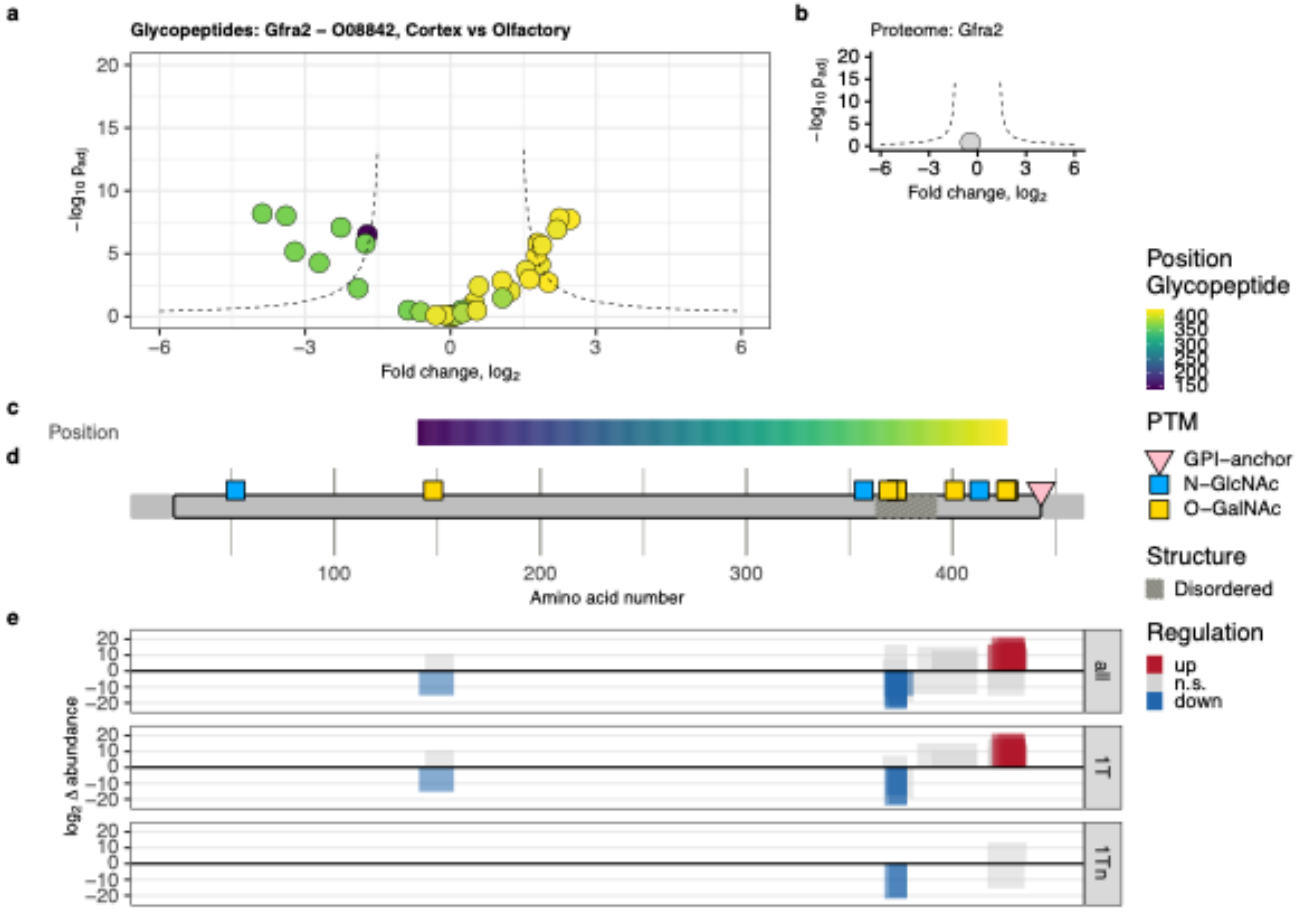

Supplementary Fig. 15. Position-specific regulation of GFRA2 O-glycosylation between cerebral cortex and olfactory bulb. (**a**) Positional volcano blot showing differential abundance of individual O-glycopeptides from GFRA2 (Uniprot O08842) between the cerebral cortex and olfactory bulb. The x-axis represents the $\log_2$ fold change, and the y-axis the $-\log_{10}$ adjusted P value. Each circle corresponds to a quantified O-glycopeptide and is color-coded according to its position within the protein sequence where modifications are localized. Dashed lines indicate significance and fold-change thresholds. (**b**) Conventional proteome volcano plot showing that the overall abundance of GFRA2 protein is not significantly altered between the two brain regions, indicating that site-specific glycosylation changes occur independently of changes in total protein abundance. (**c**) Color scale indicating the relative amino acid position of quantified O-glycopeptides along the protein sequence. (**d**) Linear schematic representation of GFRA2 protein illustrating annotated structural features including N-GlcNAc, GPI-anchor (Uniprot O08842) and mapped O-GalNAc glycosylation sites. O-glycosylation and N-glycosylation sites are shown as yellow and blue squares, respectively, the disordered region is indicated by grey hatching and the GPI-anchor attached to ω-site (S443) is shown as pink triangle. The extracellular, transmembrane and cytoplasmic regions are indicated below as color lines. (**e**) Position-resolved abundance changes of O-glycopeptides mapped onto the protein sequence. Bars represent $\log_2$ abundance changes between olfactory bulb and cerebral cortex for all quantified O-glycopeptides ("all") and for glycopeptides carrying 1T-core or 1Tn-antigen O-glycan modifications. Red indicates increased abundance, blue decreased abundance, and grey non-significant regulation. GFRA2 showed reduced levels of O-glycosylation within the distal extracellular stalk region proximal to the GPI-anchor in the olfactory bulb compared to the cerebral cortex. In contrast, O-glycopeptides mapped to the proximal region adjusted to GFRA2 D3-domain (aa 367-378) exhibited increased abundance in the olfactory bulb, demonstrating positional-specific regulation of GFRA2 O-glycosylation.

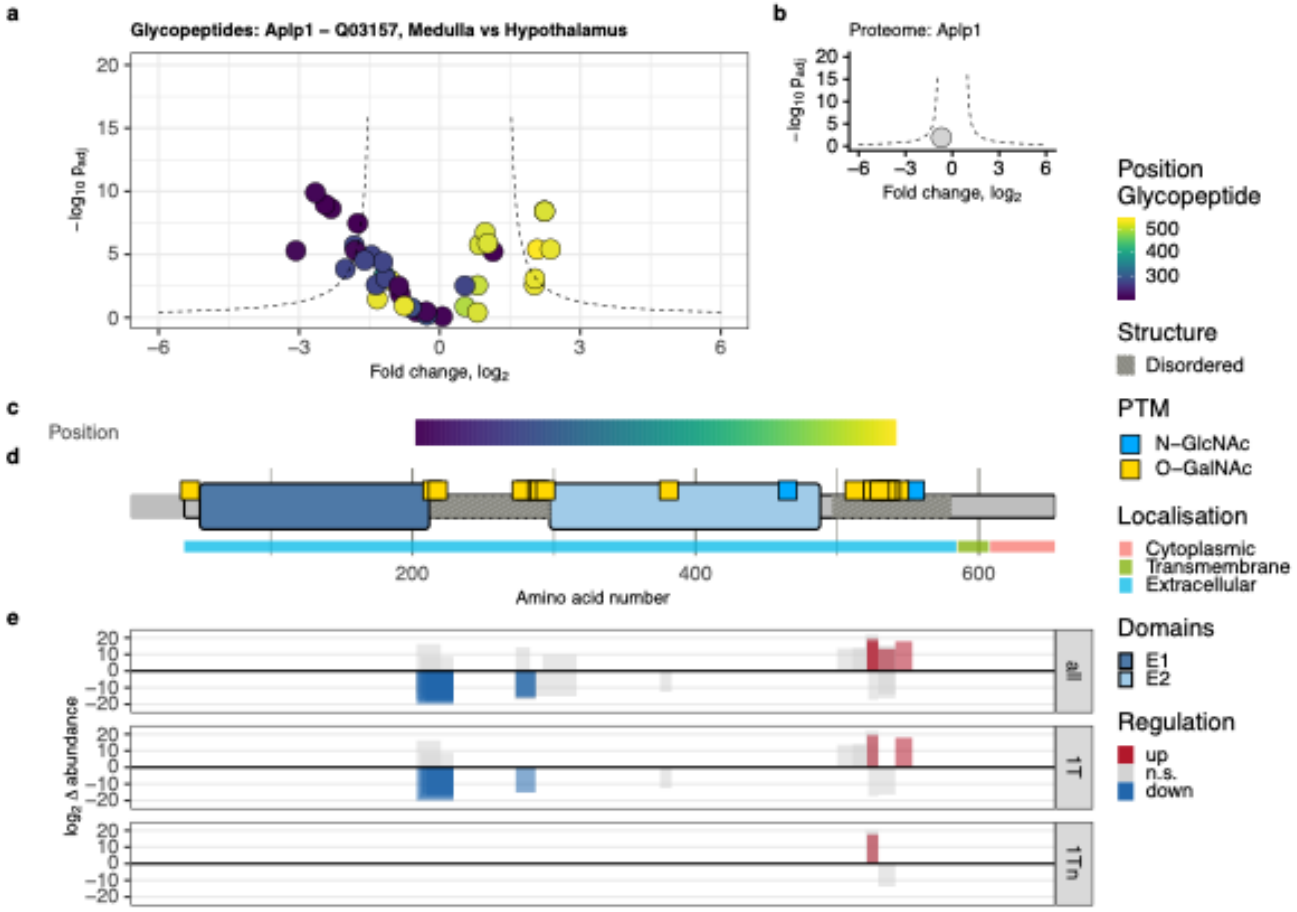

Supplementary Fig. 16. Position-specific regulation of APLP1 O-glycosylation between medulla and hypothalamus. (**a**) Positional volcano blot showing differential abundance of individual O-glycopeptides from APLP1 (Uniprot: Q03157) between the medulla and hypothalamus. The x-axis represents the $\log_2$ fold change, and the y-axis the $-\log_{10}$ adjusted P value. Each circle corresponds to a quantified O-glycopeptide and is color-coded according to its position within the protein sequence where modifications are localized. Dashed lines indicate significance and fold-change thresholds. (**b**) Conventional proteome volcano plot showing that the overall abundance of APLP1 protein is not significantly altered between the two brain regions, indicating that site-specific glycosylation changes occur independently of changes in total protein abundance. (**c**) Color scale indicating the relative amino acid position of quantified O-glycopeptides along the protein sequence. (**d**) Linear schematic representation of APLP1 protein illustrating annotated structural features including N-GlcNAc (Uniprot Q03157) and mapped O-GalNAc glycosylation sites. O-glycosylation and N-glycosylation sites are shown as yellow and blue squares, respectively, the disordered region is indicated by grey hatching. E1 and E2 domains are drawn as blue and light blue squares, respectively. The extracellular, transmembrane and cytoplasmic regions are indicated below as color lines. (**e**) Position-resolved abundance changes of O-glycopeptides mapped onto the protein sequence. Bars represent $\log_2$ abundance changes between medulla and hypothalamus for all quantified O-glycopeptides ("all") and for glycopeptides carrying 1T-core or 1Tn-antigen O-glycan modifications. Red indicates increased abundance, blue decreased abundance, and grey non-significant regulation. Our analysis of APLP1 glycosylation shows increased abundance of O-glycopeptides proximal to transmembrane domain in medulla, whereas abundance of O-glycopeptides adjacent to the E1 and E2 domains was increased in hypothalamus.

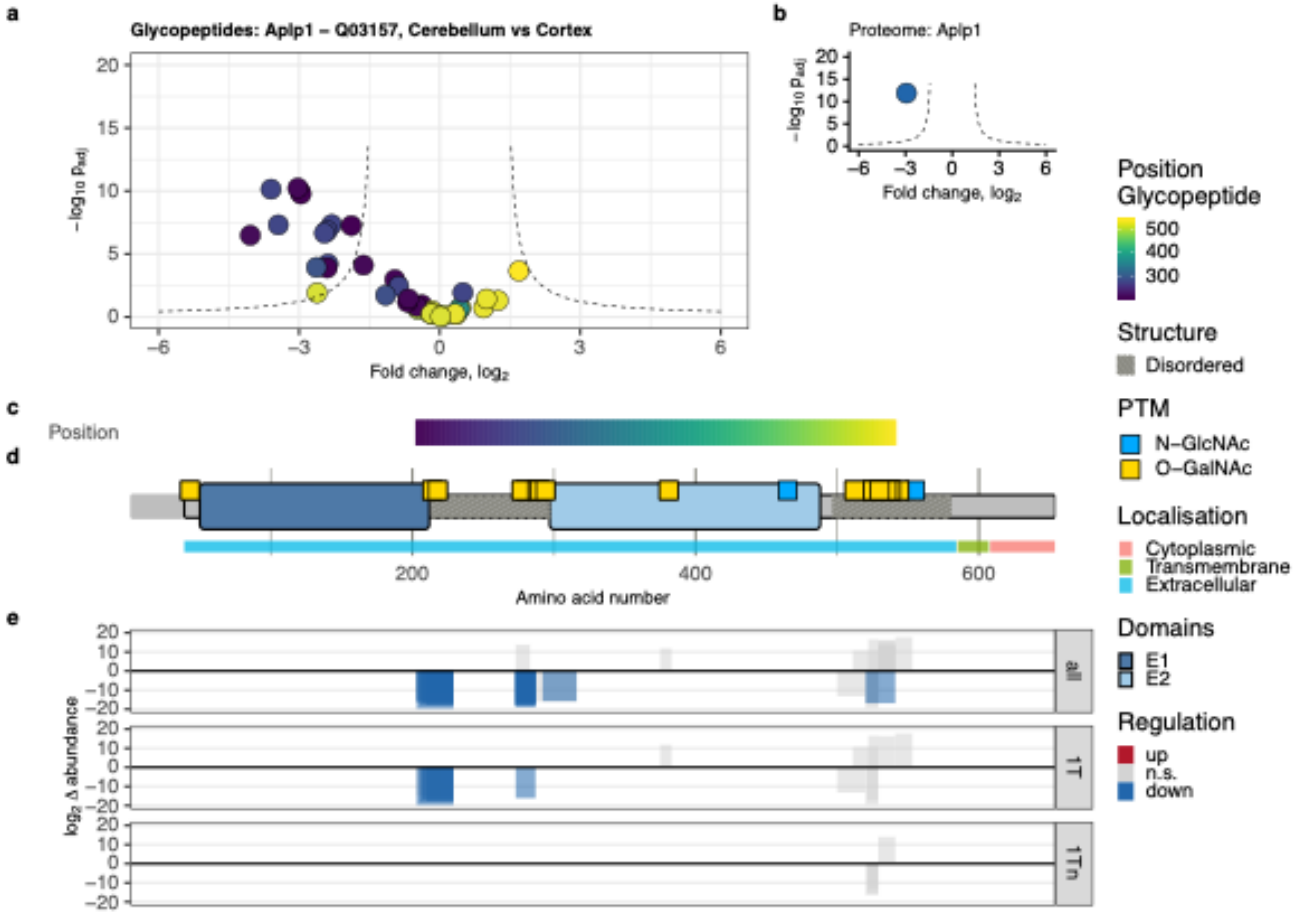

Supplementary Fig. 17. Concordant regulation of APLP1 O-glycosylation between cerebellum and cerebral cortex. (**a**) Positional volcano blot showing differential abundance of individual O-glycopeptides from APLP1 (Uniprot Q03157) between the cerebellum and cerebral cortex. The x-axis represents the $\log_2$ fold change, and the y-axis the $-\log_{10}$ adjusted P value. Each circle corresponds to a quantified O-glycopeptide and is color-coded according to its position within the protein sequence where modifications are localized. Dashed lines indicate significance and fold-change thresholds. (**b**) Conventional proteome volcano plot showing that APLP1abundance is significantly decreased in cerebellum compared to cerebral cortex, indicating region-specific differences in protein exptession. (**c**) Color scale indicating the relative amino acid position of quantified O-glycopeptides along the protein sequence. (**d**) Linear schematic representation of APLP1 protein illustrating annotated structural features including N-GlcNAc (Uniprot Q03157) and mapped O-GalNAc glycosylation sites. O-glycosylation and N-glycosylation sites are shown as yellow and blue squares, respectively, the disordered region is indicated by grey hatching. E1 and E2 domains are drawn as blue and light blue squares, respectively. The extracellular, transmembrane and cytoplasmic regions are indicated below as color lines. (**e**) Position-resolved abundance changes of O-glycopeptides mapped onto the protein sequence. Bars represent $\log_2$ abundance changes between cerebellum and cerebral cortex for all quantified O-glycopeptides ("all") and for glycopeptides carrying 1T-core or 1Tn-antigen O-glycan modifications. Blue indicates decreased abundance, and grey non-significant regulation. Our analysis of APLP1 glycosylation shows concordant decrease of protein and O-glycopeptides abundances in the cerebellum compared to the cerebral cortex across protein domains.

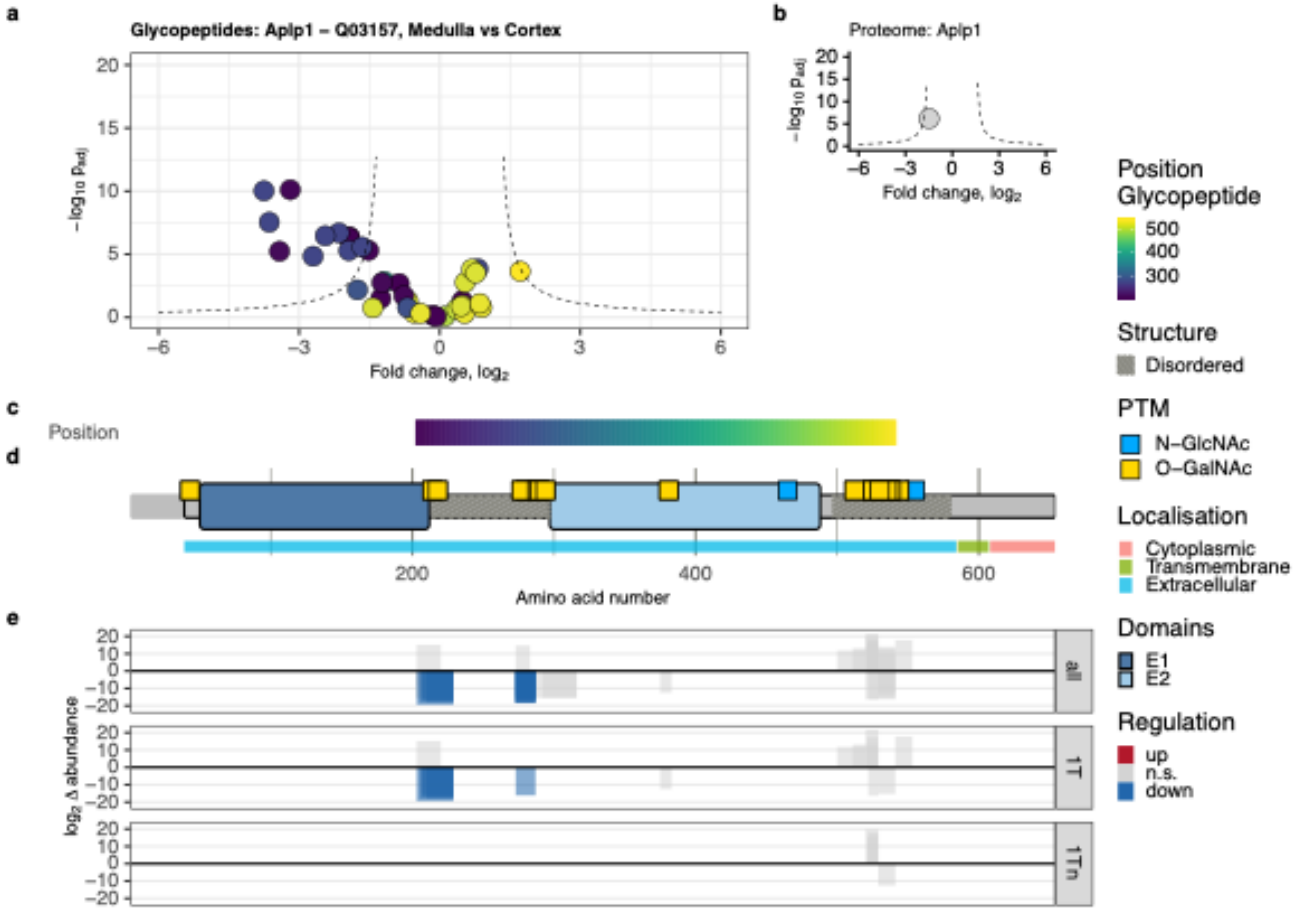

Supplementary Fig. 18. Position-specific regulation of APLP1 O-glycosylation between medulla and cerebral cortex. (**a**) Positional volcano blot showing differential abundance of individual O-glycopeptides from APLP1 (Uniprot Q03157) between the medulla and cerebral cortex. The x-axis represents the $\log_2$ fold change, and the y-axis the $-\log_{10}$ adjusted P value. Each circle corresponds to a quantified O-glycopeptide and is color-coded according to its position within the protein sequence where modifications are localized. Dashed lines indicate significance and fold-change thresholds. (**b**) Conventional proteome volcano plot showing that the overall abundance of APLP1 protein is not significantly altered between the two brain regions, indicating that site-specific glycosylation changes occur independently of changes in total protein abundance. (**c**) Color scale indicating the relative amino acid position of quantified O-glycopeptides along the protein sequence. (**d**) Linear schematic representation of APLP1 protein illustrating annotated structural features including N-GlcNAc (Uniprot Q03157) and mapped O-GalNAc glycosylation sites. O-glycosylation and N-glycosylation sites are shown as yellow and blue squares, respectively, the disordered region is indicated by grey hatching. E1 and E2 domains are drawn as blue and light blue squares, respectively. The extracellular, transmembrane and cytoplasmic regions are indicated below as color lines. (**e**) Position-resolved abundance changes of O-glycopeptides mapped onto the protein sequence. Bars represent $\log_2$ abundance changes between medulla and cerebral cortex for all quantified O-glycopeptides ("all") and for glycopeptides carrying 1T-core or 1Tn-antigen O-glycan modifications. Blue indicates decreased abundance, and grey non-significant regulation. Our analysis of APLP1 glycosylation revealed a decreased abundance of O-glycopeptides mapping to adjacent regions of the E1 and E2 domains in the medulla compared with the cerebral cortex, whereas O-GalNAc sites proximal to the transmembrane domain remain unaltered between the brain regions.

Supplementary References

1. Vakhrushev, S.Y. et al. Enhanced mass spectrometric mapping of the human GalNAc-type O-glycoproteome with SimpleCells. *Mol Cell Proteomics* **12**, 932-944 (2013).
2. Ye, Z., Mao, Y., Clausen, H. & Vakhrushev, S.Y. Glyco-DIA: a method for quantitative O-glycoproteomics with in silico-boosted glycopeptide libraries. *Nat Methods* **16**, 902-910 (2019).
3. Williams, S.E. et al. Mammalian brain glycoproteins exhibit diminished glycan complexity compared to other tissues. *Nature communications* **13**, 275 (2022).
4. Suttapitugsakul, S., Matsumoto, Y., Aryal, R.P. & Cummings, R.D. Large-Scale and Site-Specific Mapping of the Murine Brain O-Glycoproteome with IMPa. *Analytical chemistry* **95**, 13423-13430 (2023).
5. Yang, W. et al. Quantitative mapping of the in vivo O-GalNAc glycoproteome in mouse tissues identifies GalNAc-T2 O-glycosites in metabolic disorder. *Proceedings of the National Academy of Sciences of the United States of America* **120**, e2303703120 (2023).
6. Taus, T. et al. Universal and confident phosphorylation site localization using phosphoRS. *Journal of proteome research* **10**, 5354-5362 (2011).
7. UniProt, C. UniProt: the Universal Protein Knowledgebase in 2025. *Nucleic Acids Res* **53**, D609-D617 (2025).
8. Wong, H.S. et al. Cytoskeletal confinement of CX3CL1 limits its susceptibility to proteolytic cleavage by ADAM10. *Mol Biol Cell* **25**, 3884-3899 (2014).
9. Iemmolo, M., Ghersi, G. & Bivona, G. The Cytokine CX3CL1 and ADAMs/MMPs in Concerted Cross-Talk Influencing Neurodegenerative Diseases. *Int J Mol Sci* **24** (2023).
10. Eugenin, J., Eugenin-von Bernhardi, L. & von Bernhardi, R. Age-dependent changes on fractalkine forms and their contribution to neurodegenerative diseases. *Front Mol Neurosci* **16**, 1249320 (2023).
11. Schilling, S. et al. APLP1 Is a Synaptic Cell Adhesion Molecule, Supporting Maintenance of Dendritic Spines and Basal Synaptic Transmission. *J Neurosci* **37**, 5345-5365 (2017).
12. Schauenburg, L. et al. APLP1 is endoproteolytically cleaved by gamma-secretase without previous ectodomain shedding. *Sci Rep* **8**, 1916 (2018).
13. Muller, U.C., Deller, T. & Korte, M. Not just amyloid: physiological functions of the amyloid precursor protein family. *Nat Rev Neurosci* **18**, 281-298 (2017).
14. Lee, S. et al. The E2 domains of APP and APLP1 share a conserved mode of dimerization. *Biochemistry* **50**, 5453-5464 (2011).

15. Onodera, W., Asahi, T. & Sawamura, N. Rapid evolution of mammalian APLP1 as a synaptic adhesion molecule. *Sci Rep* **11**, 11305 (2021).
16. Hoefgen, S. et al. Heparin induced dimerization of APP is primarily mediated by E1 and regulated by its acidic domain. *J Struct Biol* **187**, 30-37 (2014).
17. Mao, X. et al. Aplp1 interacts with Lag3 to facilitate transmission of pathologic alpha-synuclein. *Nature communications* **15**, 4663 (2024).
18. Bigalke, J.M. et al. Cryo-EM structure of the activated RET signaling complex reveals the importance of its cysteine-rich domain. *Science advances* **5**, eaau4202 (2019).
19. Ibanez, C.F., Paratcha, G. & Ledda, F. RET-independent signaling by GDNF ligands and GFRalpha receptors. *Cell Tissue Res* **382**, 71-82 (2020).
20. Mayor, S. & Riezman, H. Sorting GPI-anchored proteins. *Nat Rev Mol Cell Biol* **5**, 110-120 (2004).
21. Liu, Y.S. & Fujita, M. Mammalian GPI-anchor modifications and the enzymes involved. *Biochem Soc Trans* **48**, 1129-1138 (2020).
22. Sandmark, J. et al. Structure and biophysical characterization of the human full-length neurturin-GFRa2 complex: A role for heparan sulfate in signaling. *The Journal of biological chemistry* **293**, 5492-5508 (2018).
23. Shurer, C.R. et al. Physical Principles of Membrane Shape Regulation by the Glycocalyx. *Cell* **177**, 1757-1770 e1721 (2019).